Lithos 224–225 (2015) 225–239

Contents lists available at ScienceDirect

Lithos

journal homepage: www.elsevier.com/locate/lithos

Thickened juvenile lower crust-derived ~90 Ma adakitic rocks in the central Lhasa terrane, Tibet

Gao-Yuan Sun [a], Xiu-Mian Hu [a,*], Di-Cheng Zhu [b,c], Wen-Tao Hong [d], Jian-Gang Wang [e], Qing Wang [b,c]

[a] State Key Laboratory of Mineral Deposits Research, School of Earth Sciences and Engineering, Nanjing University, Xianlin Dadao 163, Nanjing 210023, China
[b] State Key Laboratory of Geological Processes and Mineral Resources, China University of Geosciences, Beijing, 100083 China
[c] School of Earth Science and Resources, China University of Geosciences, Beijing 100083, China
[d] Nanjing Institute of Geology and Mineral Resources, China Geological Survey, Nanjing 210016, China
[e] State Key Laboratory of Lithospheric Evolution, Institute of Geology and Geophysics, Chinese Academy of Sciences, Beijing 100029, China

ARTICLE INFO

Article history:
Received 12 November 2014
Accepted 9 March 2015
Available online 20 March 2015

Keywords:
Adakitic rocks
Crustal thickening
Late Cretaceous
Lhasa terrane
Tibet

ABSTRACT

The questions of why the Late Cretaceous magmatism generated and how the nature of the lower crust evolves in central Tibet remain poorly constrained. In this paper, we report the presence of early Late Cretaceous adakitic rocks from the Azhang area, northern edge of the central Lhasa subterrane, central Tibet. These rocks are rhyodacites/dacites in composition and have geochemical characteristics of adakitic rocks, e.g., high Sr (554–836 ppm), Sr/Y (66–100), and $(La/Yb)_N$ (20–21), low Y (7.96–8.96 ppm) and heavy rare earth elements (HREE). In situ zircon U–Pb dating for two samples yields an early Late Cretaceous age (90 ± 1 Ma and 87 ± 1 Ma). The low MgO (1.4–1.9 wt.%) contents and compatible element abundances (e.g., Cr = 22–30 ppm; Ni = 19–25 ppm) indicate that these rocks were most likely derived from the partial melting of a garnet-bearing amphibolite under a thickened lower crust condition. The positive whole-rock $\varepsilon_{Nd}(t)$ (+2.5 to +5.6) and zircon $\varepsilon_{Hf}(t)$ (+8.9 to +16.0) values suggest that this thickened lower crust was juvenile. The crust beneath the central Lhasa subterrane may have been significantly thickened due to tectonic shortening in response to the Lhasa–Qiangtang collision and magma underplating before the emplacement of Azhang adakitic rocks (~90 Ma). We argue that regional lithospheric delamination at ~90 Ma triggered the partial melting of the lowermost garnet-bearing crust that is still attached to the middle crust to generate the Azhang adakitic rocks. The presence of the ~90 Ma Azhang adakitic rocks provides valuable constraints on the origin of the early Late Cretaceous magmatism in the central Lhasa subterrane and on the crustal evolution beneath the Lhasa–Qiangtang collisional zone prior to the Cenozoic India–Asia collision.

1. Introduction

The Tibetan Plateau is thought to be the most outstanding area for studying the deep processes operating at continent–continent collisions on Earth. As one of the main tectonic components of this plateau, the Lhasa terrane was the last continental slice accreted onto the southern margin of this plateau before the India–Asia collision (Yin and Harrison, 2000; Zhu et al., 2013). Mesozoic to Cenozoic magmatic rocks are widely exposed in the Lhasa terrane (Zhu et al., 2008a, b). Numerous studies on the southern Lhasa terrane (i.e., Cretaceous Gangdese magmatic arc) have suggested an archetype of Andean-style margin related to the northward subduction of the Neo-Tethyan Ocean prior to the Cenozoic India–Asia collision (Yin and Harrison, 2000; Ding et al., 2003; Chung et al., 2005; Chu et al., 2006; Mo et al., 2007, 2008; Ji et al., 2009). However, the generation of the Cretaceous magmatism in the central and northern Lhasa subterranes remains poorly understood, with proposed models including the northward flat/low-angle subduction of the Neo-Tethyan Ocean lithosphere (Ding et al., 2003; Kapp et al., 2007a; Ma et al., 2013a, b, c) or the southward subduction of the Bangong–Nujiang Ocean lithosphere and subsequent Lhasa–Qiangtang collision (Mo et al., 2005; Pan et al., 2006; Zhu et al., 2009a, 2011, 2013; Sui et al., 2013; Chen et al., 2014). Recent studies identified significant mantle contribution in the Early Cretaceous magmatic rocks along the Lhasa–Qiangtang collision zone and attributed such contribution to the result of slab break-off of the Bangong–Nujiang Ocean lithosphere (Zhu et al., 2009a, 2011; Sui et al., 2013; Chen et al., 2014). Several studies on the Late Cretaceous potassium-rich and magnesium-rich volcanic rocks from the Lhasa–Qiangtang collision zone indicate that the crust of this region may have been thickened prior to the eruption of such volcanic rocks (Yu et al., 2011; Li et al., 2013; Wang et al., 2014). Nevertheless, such recognition must be validated with more lines of evidence from petrological, geochemical, and geochronological data, not only from the northern Lhasa subterrane, but also from the central Lhasa subterrane.

* Corresponding author. Tel.: +86 25 89683002.
E-mail address: huxm@nju.edu.cn (X.-M. Hu).

http://dx.doi.org/10.1016/j.lithos.2015.03.010
0024-4937/

Several hypotheses have been proposed to explain the generation of adakitic rocks (Castillo, 2012, and references therein). In particular, the thickened lower crust-derived adakitic rocks within the interior of a continental setting have generally been considered as an indicator for crust thickening, providing important insights into crustal evolution and the associated deep crust–mantle interaction (Atherton and Petford, 1993; Petford and Atherton, 1996; Xu et al., 2002; Wang et al., 2004a, b, 2005, 2006a, b). In this paper, we report the presence of the early Late Cretaceous Azhang adakitic rocks in the central Lhasa subterrane, central Tibet (Fig. 1c). Whole-rock geochemical, Sr–Nd–Pb isotopic and in situ zircon U–Pb dating and Hf isotopic data indicate that these rocks were most likely derived from the partial melting of a thickened juvenile lower crust. Our finding of the Azhang adakitic rocks in the central Lhasa subterrane provides valuable constraints on the origin of the Late Cretaceous magmatism in the central Lhasa subterrane and on the evolution of lower crust underneath the Lhasa–Qiangtang collisional zone prior to the Cenozoic India–Asia collision.

2. Geological background

The Tibetan Plateau is composed of several terranes, including the Tethyan Himalaya, Lhasa terrane, Qiangtang terrane, and Songpan–Ganzi complex from the south to north (Fig. 1a, Yin and Harrison, 2000). The Lhasa terrane is located in the southern portion of this plateau and is separated from the Tethyan Himalaya to the south by the Yarlung–Zangbo suture zone and from the Qiangtang terrane to the north by the Bangong–Nujiang suture zone (Fig. 1a, Yin and Harrison, 2000; Zhu et al., 2013). This terrane can be divided into three domains: southern, central, and northern Lhasa subterranes according to the differences of crustal nature and sedimentary covers (Fig. 1b), separated by the Luobadui–Milashan Fault (LMF) and the Shiquan River–Nam Tso Mélange Zone (SNMZ), respectively (Zhu et al., 2009a, 2011, 2013).

The southern Lhasa subterrane is characterized by the presence of the widespread Cretaceous–Early Tertiary Gangdese batholiths and Paleogene Linzizong volcanic rocks (Chu et al., 2006; Mo et al., 2007, 2008; Wen et al., 2008; Ji et al., 2009; Zhu et al., 2013) with minor sedimentary covers. These rocks were commonly considered to be associated with the northward subduction of the Neo-Tethyan Ocean lithosphere and subsequent India–Asia collision (Yin and Harrison, 2000; Ding et al., 2003; Chung et al., 2005; Mo et al., 2007, 2008). A Carboniferous metasedimentary sequence, Permian limestone, minor Jurassic siliciclastic rocks and abundant Cretaceous intrusive and volcanic rocks are exposed in the central Lhasa subterrane (Ding and Lai, 2003; Zhou et al., 2008; Zhu et al., 2009a, 2011, 2013, and references therein). Cretaceous strata with thicknesses up to several thousands of meters crop out on the central Lhasa subterrane; these strata include the Lower Cretaceous Duoni sedimentary-volcanic rocks and Langshan limestone, and Upper Cretaceous Jingzhushan and Daxiong conglomerates (Leeder et al., 1988; Yin et al., 1988; Zhang et al., 2012; Sun et al., in press). Previous studies argued that the Cretaceous magmatism in this

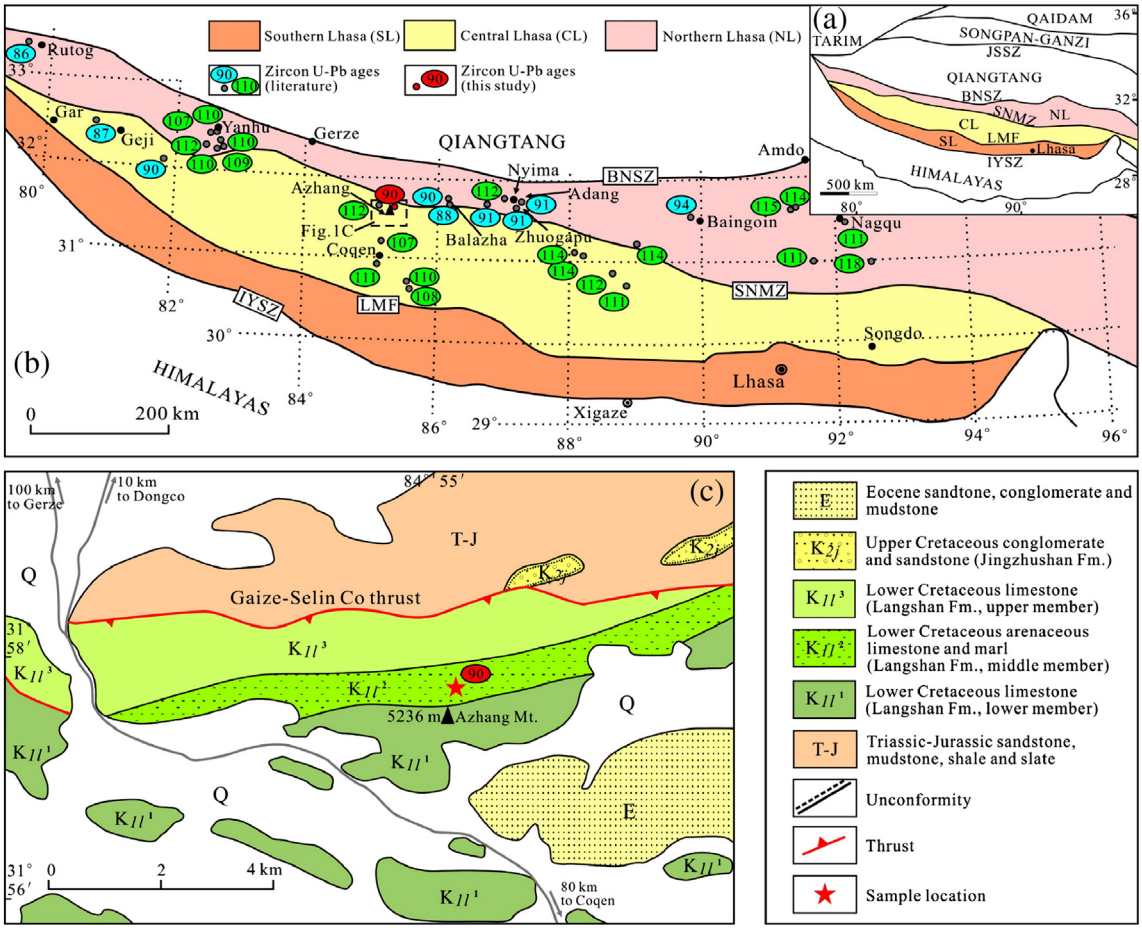

Fig. 1. (a) Tectonic framework of the Tibetan plateau (Zhu et al., 2009a). (b) Tectonic units of the Lhasa terrane showing the major subdivisions and distributions of magmatic rocks dated at ~110 Ma and ~90 Ma. Literature data are from Zhu et al. (2009a, 2011), Sui et al. (2013), Qu et al. (2006), Ma and Yue (2010), Yu et al. (2011), Huang et al. (2013), Wang et al. (2014) and Li et al. (2014). (c) Geological map of the Azhang mountain area, north of Coqen, modified after Liu et al. (2004). BNSZ = Bangong–Nujiang suture zone; IYSZ = Yarlung–Zangbo suture zone; SNMZ = Shiquan River–Nam Tso Mélange Zone; LMF = Luobadui–Milashan Fault; Fm. = Formation; Mt. = Mountain.

subterrane is associated with the northward subduction of the Neo-Tethyan Ocean lithosphere (Harris et al., 1990; Zhang et al., 2004), but new geochemical and geochronological data led Zhu et al. (2009a, 2011) to propose that they were most likely associated with the southward subduction of the Bangong–Nujiang Ocean lithosphere. The rock units in the northern Lhasa subterrane are mainly composed of abundant Cretaceous volcano-sedimentary rocks with secondary Middle Triassic and Upper Jurassic sequences (Pan et al., 2004, 2012; Zhu et al., 2013).

Zhu et al. (2011, 2013) asserted that the central Lhasa subterrane was once a micro-continent with Proterozoic–Archean basement, while the southern and northern Lhasa subterranes (excluding the Amdo micro-continent) are characterized by the presence of juvenile lower crust. Geological mapping and structural restoration indicated that the Lhasa terrane experienced strong crustal deformation and shortening during the mid-Late Cretaceous prior to the India–Asia collision (Pan, 1993; Murphy et al., 1997; Kapp et al., 2007a; Volkmer et al., 2007).

3. Field occurrence and petrography

The Azhang adakitic rocks investigated in this study (GPS: 31°57′49.3″N, 84°57′59.8″E; 4830 m) are exposed in the northern edge of the central Lhasa subterrane, approximately 80 km north of Coqen (Fig. 1b). In this region, thick Cretaceous strata are well outcropped, consisting of the Lower-mid Cretaceous Langshan Formation and the Upper Cretaceous Jingzhushan Formation (XZBGM, Xizang Bureau of Geology (1993; Liu et al., 2004). The Langshan Formation can be further subdivided into three members (Fig. 1b). The lower and upper members are composed of *Orbitolina*-bearing limestones and the middle member comprises marls interbedded with arenaceous limestone. The Jingzhushan Formation unconformably overlies the underlying strata and comprises terrestrial conglomerates and sandstones. Sedimentology studies suggested that the Langshan Formation was deposited in the lagoon and reefal environments (Zhang et al., 2000, 2004; Scott et al., 2010), while the Jingzhushan Formation were deposited in an alluvial fan setting and most likely recorded the history of uplift and erosion of the central-northern Lhasa subterrane (Zhang et al., 2012; Sun et al., in press).

The Azhang adakitic rocks are exposed in conformable contact with the arenaceous limestone and marls of the middle member of the Langshan Formation (Fig. 1c, Fig. 2a). These adakitic rocks extend along east–west trends and have three layers with thicknesses of 2 m, 1.5 m and 0.8 m. These samples are all in green color and display porphyritic textures (Fig. 2a). The phenocrysts are composed mostly of plagioclase (~10–15%, Fig. 2b) with polysynthetic twinning. The matrix shows pilotaxitic texture and consists of microcrystal plagioclase (~65%), quartz (~15–20%), magnetite (~5%), and minor apatite, zircon, and glass.

4. Analytical methods and results

4.1. Zircon U–Pb age data

The descriptions of the analytical methods are presented in Appendix A. Representative Cathodoluminescence (CL) images of zircons are shown in Fig. 3 and the data are given in Appendix B-Table 1. A total of forty-five zircons from two samples (LS-P and LS-74) are mostly 100–150 μm in size and euhedral to subhedral with an aspect ratio of 2:1–4:1(Fig. 3). All of the zircons show homogeneous texture in CL images, and none of them contain inherited cores. Most of these zircons have weak to moderate oscillatory-zone and/or hourglass-structure (Fig. 3). These characteristics, together with their high Th/U ratios (0.82–1.74), suggest a magmatic origin (Hoskin and Schaltegger, 2003).

All the analyses fall on the concordant curve (Fig. 3). Twenty-four analyses from sample LS-P show $^{206}Pb/^{238}U$ ages between 88 ± 2 Ma to 92 ± 2 Ma, with a weighted mean age of 90 ± 1 Ma (MSWD [mean square weighted deviation] = 0.22, n = 24). Twenty-one analyses from sample LS-74 show similar $^{206}Pb/^{238}U$ ages, with a weighted mean age of 87 ± 1 Ma (MSWD = 0.33, n = 21). These age data suggest that the samples were emplaced in the early Late Cretaceous, which is time-equivalent with the Balazha porphyries (ca. 90–88 Ma, ~50 km east of Azhang) and Zhuogapu Mg-rich volcanic rocks (ca. 91 Ma, ~250 km east of Azhang) (Fig. 1b) (Yu et al., 2011; Wang et al., 2014). Our age data are a bit younger than the Langshan Formation (e.g., ~113–96 Ma, Scott et al., 2010; Sun et al., in press), indicating that the Azhang adakitic rocks were emplaced as sills (dacite/rhyolite porphyry) within the Langshan Formation.

4.2. In situ zircon Hf isotopic data

In situ zircon Hf isotopic analytical methods are given in Appendix A. Forty-five zircons that have been dated from samples LS-P and LS-74 were analyzed for Hf isotopic determination (Fig. 4, Appendix B-Table 2). The $^{176}Hf/^{177}Hf$ ratios of these zircons range between 0.282973 and 0.2831713, with $\varepsilon_{Hf}(t)$ values ranging from +8.9 to +16.0. These values are close to the depleted mantle at that time (t = 90 Ma, $\varepsilon_{Hf}(t)_{DM}$ = ~+16, Bizzarro et al., 2003) and far away from those of the ancient central Lhasa basement (Zhu et al., 2011, and references therein). The Hf isotope crust model ages (T^C_{DM}) range from 130 Ma to 586 Ma.

4.3. Whole-rock major and trace element data

Whole-rock major and trace elemental analytical methods are presented in Appendix A. Whole-rock major and trace element data are listed in Appendix B-Table 3. The contents of loss on ignition (LOI) of these samples are between 2.6–4.0 wt.%, reflecting varying degrees of alteration. However, some major elements (e.g., Mg, Fe, and P),

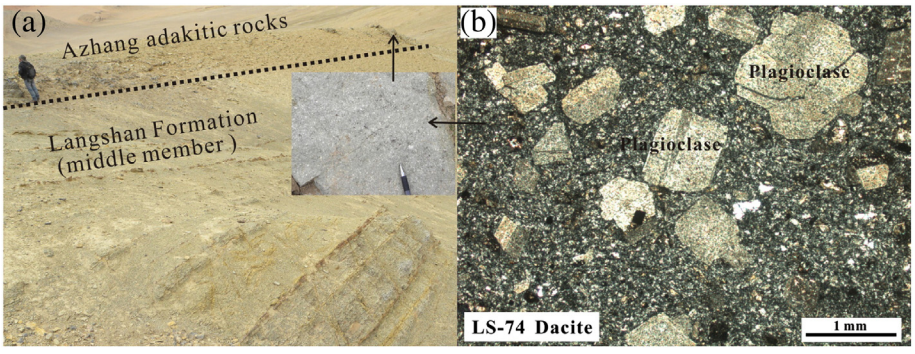

Fig. 2. (a) Field photograph showing the outcrops of Azhang adakitic rocks in the Langshan Formation (middle Member). (b) Microphotograph of the adakitic rock (sample LS-74) exhibiting porphyritic texture. (For interpretation of the references to color in this figure legend, the reader is referred to the web version of this article.)

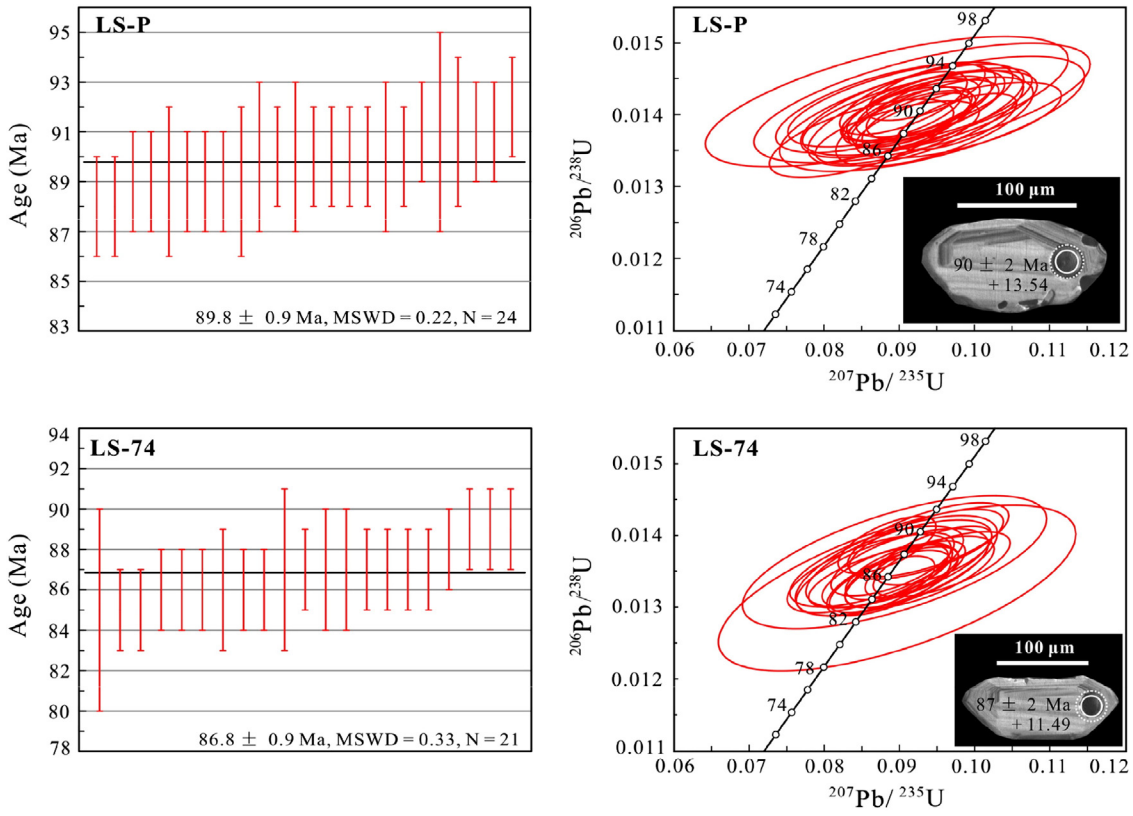

Fig. 3. Weighted mean ages, concordia diagrams of the zircons from Azhang adakitic rocks (samples LS-P and LS-74) and cathodoluminescence (CL) images of the representative zircon grains. The solid and dashed circles indicate the plots of LA-ICP-MS U–Pb dating and Hf analyses, respectively. MSWD = mean square weighted deviation.

transitional elements (e.g., Cr, Ni), and high field strength elements (HFSEs, e.g., Ti, Y, Nb, Hf) generally show poor correlations with LOI (not shown), and no clear correlations are observed between U, Pb abundances, $(^{87}Sr/^{86}Sr)_t$ ratios and LOI contents of these samples (Fig. 5), indicating that these major and trace elements are not significantly affected by alteration (Wang et al., 2006a). Therefore, high field strength elements (HFSEs), rare earth elements (REE), whole-rock Sr–Nd–Pb and zircon Hf isotopic data, as well as transitional elements are used in the following discussions.

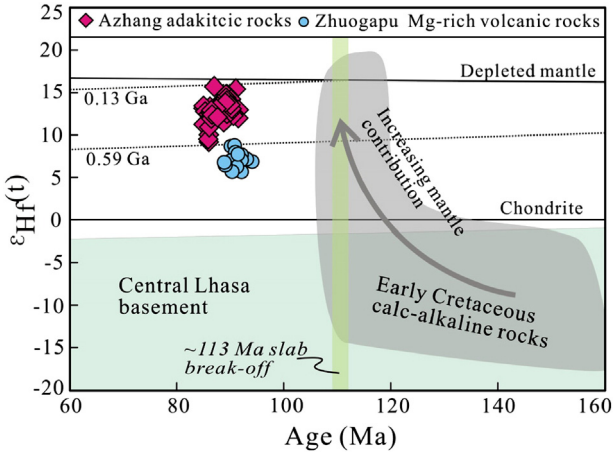

Fig. 4. Plots of $\varepsilon_{Hf}(t)$ values vs. the U-Pb age of zircons from Azhang adakitic rocks. The data of the Lhasa basement and central-northern Lhasa magmatic rocks are from Sui et al. (2013), Chen et al. (2014), Zhu et al. (2009a, 2011), and references therein. Zhuogapu Mg-rich volcanic rocks are referred to Wang et al. (2014).

All of the 10 samples analyzed have uniform major elemental compositions, and fall into the field of rhyodacite/dacite on the SiO_2 vs. Zr/TiO_2 discrimination diagram (Fig. 6a), which is effective for altered rocks (Winchester and Floyd, 1977). On the Th vs. Co classification diagram (Hastie et al., 2007), these samples fall into the field of dacite/rhyolite with calc-alkaline affinity (Fig. 6b). They have geochemical signatures similar to adakites (Defant and Drummond, 1990), e.g., high Al_2O_3 (16.4–17.2 wt.%), high Sr (554–836 ppm), and low heavy rare earth elements (HREEs) (e.g., Yb = 0.86–0.94 ppm; Y = 7.96–8.96 ppm), high Sr/Y (66–100), and $(La/Yb)_N$ ratios (20–21) (where the subscript N indicates chondrite-normalized).

These samples have low MgO (1.4–1.9 wt.%) and compatible element Cr (22–30 ppm) and Ni (19–25 ppm) contents, with $Mg^{\#}$ values of 49–55 [$Mg^{\#} = 100 * Mg/(Mg + TFe^{2+})$]. On the chondrite-normalized REE patterns (Fig. 7a), these samples show slightly negative to positive Eu anomalies ($Eu/Eu^* = 0.8–1.2$). On the primitive mantle-normalized trace element spidergrams (Fig. 7b), they are enriched in large ion lithophile elements (LILEs, such as Th and Rb) and depleted in Nb, Ta, Ti, and P, similar to those of the coeval Balazha adakitic porphyries in the northern Lhasa subterrane (Yu et al., 2011).

4.4. Whole-rock Sr–Nd–Pb isotopic data

Whole-rock Sr–Nd–Pb isotopic analytical methods and results are given in Appendix A and Appendix B-Table 3. All the initial Sr and Nd isotopic ratios are calculated at ~90 Ma. These samples show initial $^{87}Sr/^{86}Sr$ values of 0.7054–0.7062 and $\varepsilon_{Nd}(t)$ values of +2.5 to +5.6, with Nd isotope two-stage model ages (T_{DM}^{C}) of 0.44–0.69 Ga. On the $(^{87}Sr/^{86}Sr)_t$ vs. $\varepsilon_{Nd}(t)$ diagram (Fig. 8a), most of the samples plot close

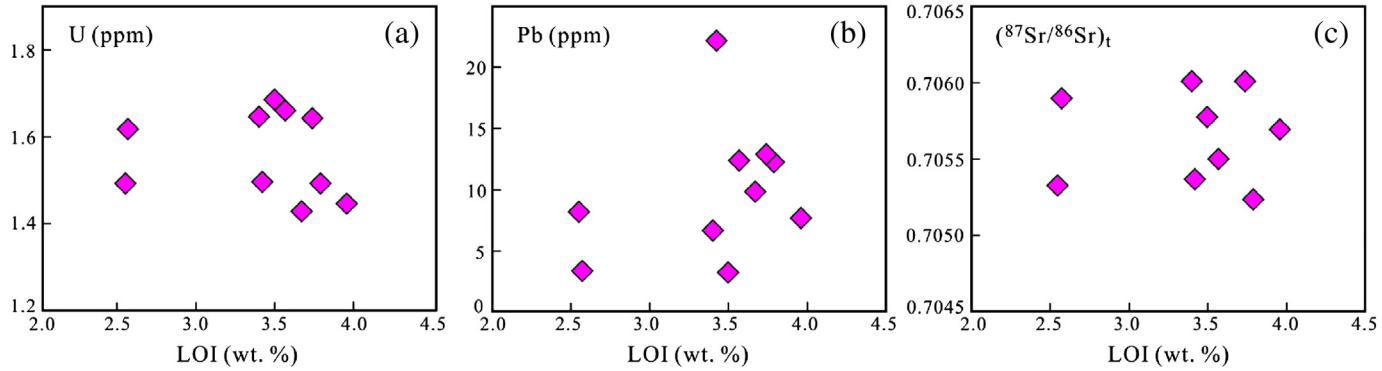

Fig. 5. LOI (loss on ignition) vs. U, Pb, $(^{87}Sr/^{86}Sr)_t$ diagrams for the Azhang adakitic rocks.

to the field of the mid-ocean ridge basalt (MORB) from the Bangong–Nujiang suture zone (Qiu, 2002; Qiu et al., 2007), but show higher $\varepsilon_{Nd}(t)$ values compared to the coeval Adang basaltic rocks (Ma and Yue, 2010) and Zhuogapu Mg-rich volcanic rocks (Wang et al., 2014).

The Azhang adakitic rocks display $^{206}Pb/^{204}Pb$ of 18.56–18.90, $^{207}Pb/^{204}Pb$ of 15.58–15.61, and $^{208}Pb/^{204}Pb$ of 38.63–39.01. On the $^{206}Pb/^{204}Pb$ vs. $^{207}Pb/^{204}Pb$ diagram (Fig. 8b), these samples plot between the MORB from the Bangong–Nujiang suture zone and Early Cretaceous arc-setting basalts, paralleling the modern MORB.

5. Discussion

5.1. Tectonic setting of the Late Cretaceous Azhang adakitic rocks

It is generally accepted that the Lhasa–Qiangtang collision occurred in the Late Jurassic to Early Cretaceous (Yin and Harrison, 2000; Kapp et al., 2005; Zhu et al., 2009a, 2011, 2013). Since then, the Lhasa–Qiangtang collisional zone could have stepped into an intracontinental setting. Geological and geochemical observations allow us to understand such tectonic settings of the central-northern Lhasa subterrane during the Late Cretaceous. For example, the syn-tectonic Late Cretaceous terrestrial molasses of the Jingzhushan and Daxiong formations (~96–91 Ma) unconformably overlie the marine Langshan limestone (DeCelles et al., 2007; Zhang et al., 2012; Sun et al., in press) in the central-northern Lhasa subterrane. Such a sedimentary transition, together with the regional petrological studies (Zhu et al., 2009a, 2011), suggest that the Lhasa–Qiangtang collision zone may have finally been amalgamated and subsequently experienced significant tectonic shortening (~50% shortening) during the development of the regional deformation and angular unconformity (Pan, 1993; Murphy et al., 1997; Volkmer et al., 2007; Kapp et al., 2005, 2007a, b; Pullen et al., 2008; Wang et al., 2014).

In addition, the ~90 Ma Adang basaltic rocks from Nyima have geochemical characteristics similar to the within-plate basalts (Ma and Yue, 2010; Wang et al., 2014) and coeval ~90 Ma Mg-rich and adakitic rocks from Nyima may have been associated with the local lithospheric delamination beneath the Lhasa–Qiangtang collision zone (Yu et al., 2011; Wang et al., 2014). In this case, the coeval Azhang adakitic rocks exposed in the northern edge of the central Lhasa subterrane (Fig. 1b) are most likely emplaced at a post-collisional setting after the final Lhasa–Qiangtang amalgamation.

5.2. Petrogenesis of the Azhang adakitic rocks

The term “adakite” implies distinct geochemical features (including high Sr and low Y and Yb contents, with high Sr/Y and La/Yb ratios), and the rocks are commonly thought to be generated by the melting of a basaltic source under an amphibolite facies to garnet-bearing amphibolite or eclogite facies with garnet ± hornblende as a residual phase (Martin et al., 2005). These rocks are originally associated with the partial melting of a hydrous subducted young oceanic lithosphere (Defant and Drummond, 1990; Kay et al., 1993). Subsequent studies have proposed

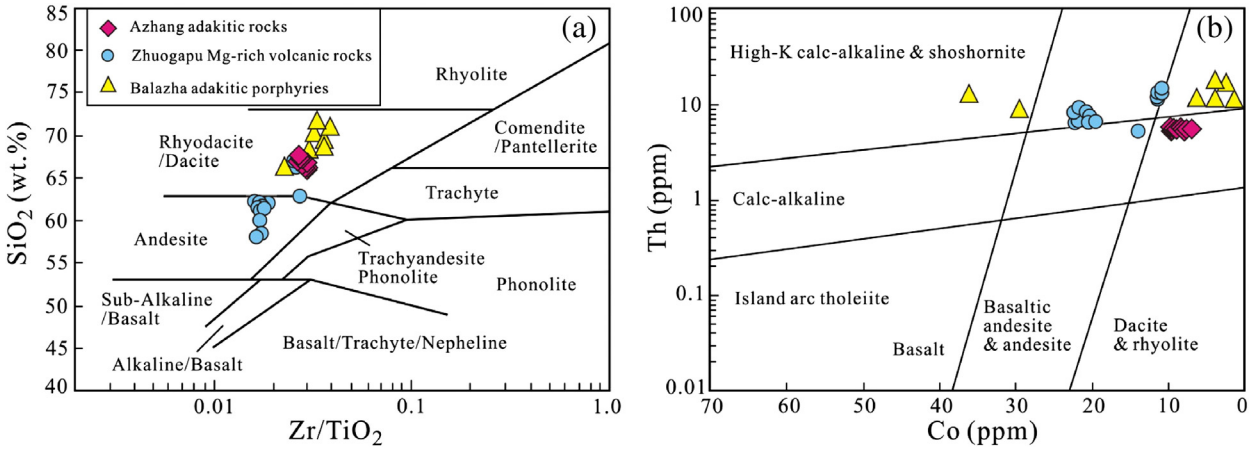

Fig. 6. (a) Plots of SiO_2 vs. Zr/TiO_2 after Winchester and Floyd (1977). (b) Th–Co diagram showing sample compositional variations after Hastie et al. (2007). Date sources: Balazha adakitic porphyries are from Yu et al. (2011); Zhuogapu Mg-rich volcanic rocks are from Wang et al. (2014).

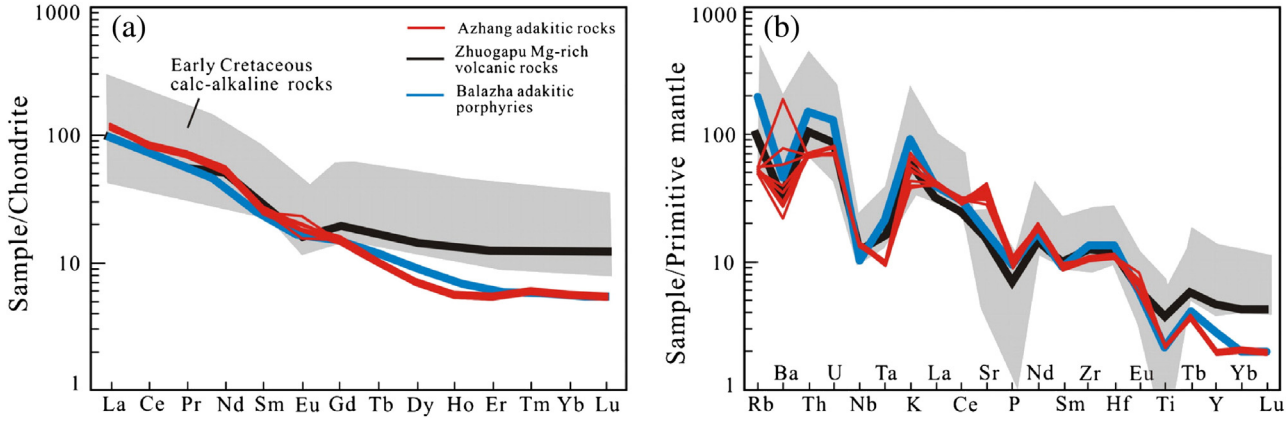

Fig. 7. (a) Chondrite-normalized REE patterns, and (b) primitive mantle-normalized trace element patterns of the Azhang adakitic rocks. Data for normalization and plotting are from Sun and McDonough (1989).
Date sources: Early Cretaceous calc-alkaline rocks are from Zhou et al. (2008); Zhu et al. (2009a, 2011) and references therein; Balazha adakitic porphyries and Zhuogapu Mg-rich volcanic rocks are from Yu et al. (2011) and Wang et al. (2014).

that several mechanisms can also account for the generation of adakites or adakitic rocks (see Castillo, 2012, and references therein). For example, partial melting of a (delaminated) thickened lower crust is able to produce adakitic rocks in the interior of a continental setting (Atherton and Petford, 1993; Petford and Atherton, 1996; Topuz et al., 2005; Castillo, 2006; Zhao et al., 2008; Xu et al., 2002; Wang et al., 2004a, b, 2005, 2006a, b). Partial melting of a stalled (or dead) oceanic slab or processes involving basaltic magma assimilation and fractional crystallization (AFC) can also account for the generation of adakitic rocks (Wang et al., 2006a; Castillo et al., 1999).

We consider that the Azhang adakitic rocks are not likely to be the products of basaltic magma AFC processes, because the coeval basaltic and intermediate lavas in the northern Lhasa subterrane have much lower $\varepsilon_{Nd}(t)$ values (Fig. 8a, Ma and Yue, 2010; Wang et al., 2014). In addition, the Azhang adakitic rocks have a depleted isotopic nature, which is inconsistent with upper crustal contamination of the central Lhasa subterrane that should lower the $\varepsilon_{Nd}(t)$ values of their primitive melts and elevate their HFSEs and SiO_2 contents (Parrish and Hodges, 1996; Harrison et al., 1999). Instead, on the La vs. $\varepsilon_{Nd}(t)$ and SiO_2 vs. $\varepsilon_{Nd}(t)$ diagrams (Fig. 9a, b), these samples show nearly horizontal trends, suggesting that the effects of crustal contamination are most likely negligible.

Strong–medium incompatible element contents and ratios can be applied to identify partial melting processes (Allègre and Minster, 1978). On the plots of La/Nb vs. La and Th/Nb vs. Th (Fig. 9c, d), the Azhang adakitic rocks exhibit well-defined linear trends, suggesting that a partial melting process plays an important role in their generation. Therefore, it is most likely that the generation of the Azhang adakitic rocks was controlled by varying degrees of partial melting of a magma source region, instead of the AFC processes.

On the chondrite-normalized REE patterns (Fig. 7a), the Azhang adakitic rocks exhibit a steep REE pattern with low Yb abundances, which could be considered as the REE fractionation during the partial melting processes, such as the heavy REE retention in the residual amphibole or garnet (Kay et al., 1993; Martin et al., 2005). The discernable concave-upward middle REE-depleted patterns of these samples indicate that they could be derived from the partial melting of lower mafic crust under varying water fugacity, leaving an amphibole-rich residue (Petford and Atherton, 1996). The absence of significant negative Eu anomalies and high Sr contents suggests a plagioclase-free source. On

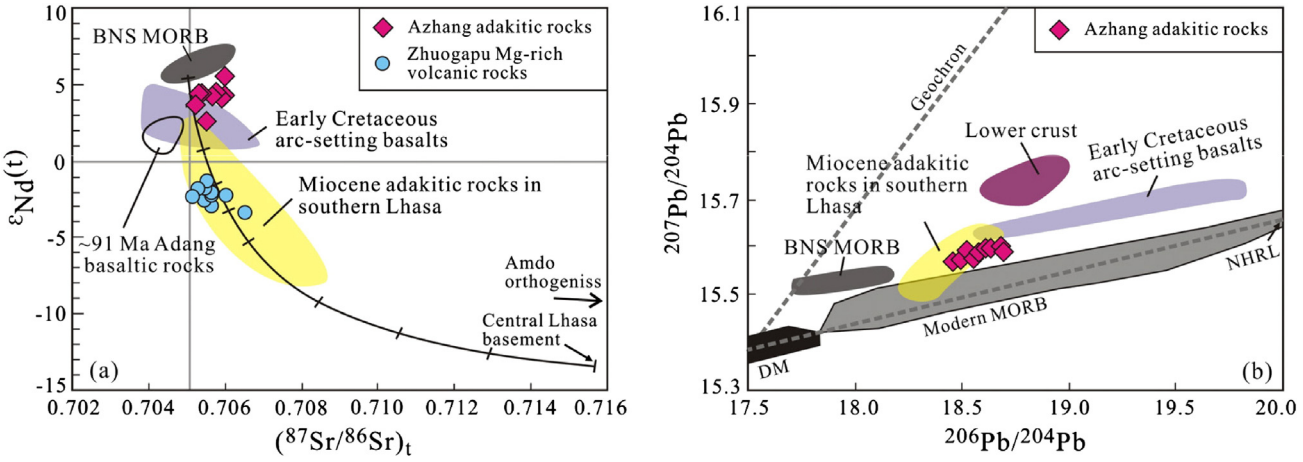

Fig. 8. (a) Plots of $(^{87}Sr/^{86}Sr)_t$ vs. $\varepsilon_{Nd}(t)$ diagram, and (b) plots of $^{207}Pb/^{204}Pb$ vs. $^{206}Pb/^{204}Pb$ of the Azhang adakitic rocks.
Date sources: MORB in the Bangong-Nujiang suture zone are from Qiu (2002), Qiu et al. (2007); Early Cretaceous arc-setting basalts are from Zhu et al. (2006) and Sui et al. (2013); Miocene adakitic rocks in southern Lhasa subterrane are from Hou et al. (2004); ancient central Lhasa basement is from Zhu et al. (2011); Amdo orthogneiss is from Miller et al. (1999); Pb isotopes of lower crust are from Lai et al. (2008).

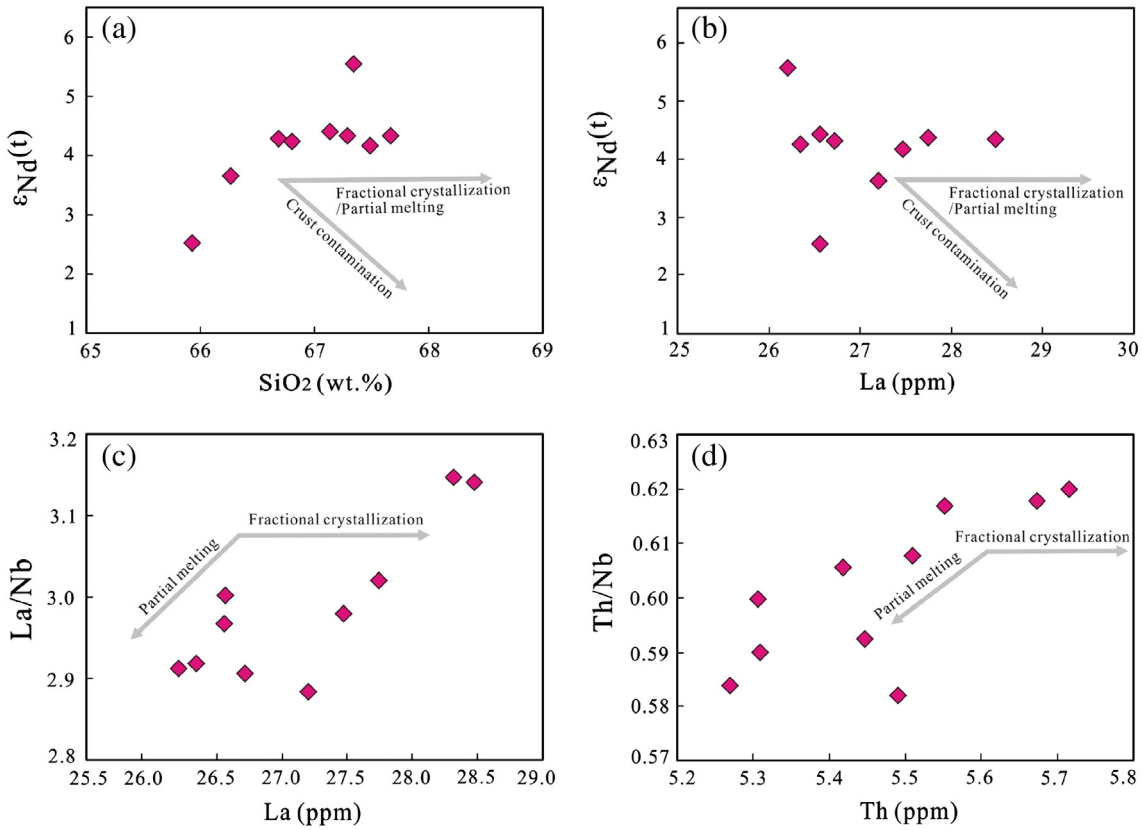

Fig. 9. (a–b) SiO_2 and La vs. $\varepsilon_{Nd}(t)$ diagrams, and (c–d) La/Nb vs. La and Th/Nb vs. Th diagrams for Azhang adakitic rocks.

the plots of Yb_N vs. $(La/Yb)_N$ and Y vs. Sr/Y (Fig. 10), the Azhang adakitic rocks fall far away from the partial melting line of eclogite, and distribute between the partial melting lines of 10% garnet-amphibolite and amphibolites, indicating that the source protoliths were likely the garnet-bearing amphibolites, rather than the pure eclogite. Therefore, it seems likely that there are at least two possible magma sources for generating the Azhang adakitic rocks, including subducted oceanic slab or (delaminated) thickened lower crust.

The depleted Nd–Hf isotopic compositions of the Azhang adakitic rocks seem likely to be derived from the subducted oceanic slab (Defant and Drummond, 1990). Given that the Azhang adakitic rocks were most likely emplaced within an intracontinental setting following the final Lhasa–Qiangtang amalgamation, the subducted Bangong–Nujiang Ocean lithosphere is unlikely to be involved in their generation. Another possibility is that the northward subducted Neo-Tethyan Ocean lithosphere would serve as a potential source candidate. However, we note that the Azhang adakitic rocks were emplaced at approximately 400 km to north of the Yarlung–Zangbo suture zone during the Late Cretaceous when the ~50% crustal shortening of the Lhasa terrane is considered to have occurred (Pan, 1993; Murphy et al., 1997; Kapp et al., 2007a, b; Volkmer et al., 2007). Such a large distance implies that the Neo-Tethyan Ocean lithosphere should have been subducted with a flat/low angle (Zhang et al., 2004; Kapp et al., 2005, 2007a; Ma et al., 2013a, b, c). However, this geodynamic regime makes it difficult to interpret the presence of Cretaceous magmatism on the southern-central Lhasa subterrane (Wen et al., 2008; Ji et al., 2009; Zhu et al.,

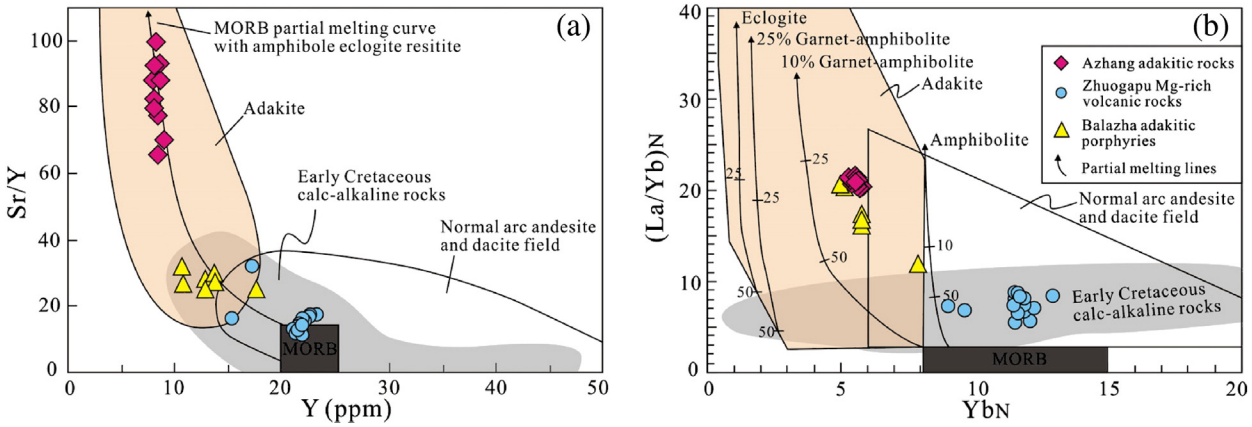

Fig. 10. (a) Plots of Sr/Y vs. Y (Defant and Drummond, 1990), and (b) $(La/Yb)_N$ vs. Yb_N (Drummond and Defant, 1990).
Date sources: Early Cretaceous calc-alkaline rocks are from Zhou et al. (2008); Zhu et al. (2009a, 2011) and references therein. Balazha adakitic porphyries and Zhuogapu Mg-rich volcanic rocks are from Yu et al. (2011) and Wang et al. (2014).

2009a, 2011, and references therein) as discussed in detail by Zhu et al. (2009a). Even though the hypothesis of the northward subduction system is feasible, the low MgO (1.4–1.9 wt.%), Cr (22–30 ppm), and Ni (19–25 ppm) contents indicate that the Azhang adakitic rocks are unlikely generated by partial melting of the subducted Neo-Tethyan Ocean lithosphere or a stalled (or dead) oceanic lithosphere as proposed elsewhere (Wang et al., 2006a). The reason is that the melts generated in this way generally have elevated MgO, Cr, and Ni contents due to their interaction with the overlying mantle peridotite during magma ascent (e.g., Cr > 30 ppm, Martin, 1999; Richards and Kerrich, 2007; Zhu et al., 2009b). Collectively, it is reasonable to exclude the possibility that the Neo-Tethyan oceanic slab produced the ~90 Ma Azhang adakitic rocks.

An alternative possibility for the generation of the Azhang adakitic rocks could be derived from the partial melting of a delaminated or thickened lower crust. In most cases, melts derived from a delaminated thickened lower crust would also interact with the overlying mantle peridotite during magma ascent, resulting in elevation of the MgO and compatible element contents (Xu et al., 2002; Wang et al., 2004a; Castillo, 2006). For the Azhang adakitic rocks, their lower Cr, Ni, and MgO contents, compared to the coeval delamination-related Balazha adakitic porphyries and Zhuogapu Mg-rich volcanic rocks in the northern Lhasa subterrane (Fig. 11, Yu et al., 2011; Wang et al., 2014) and other adakitic rocks from delaminated thickened lower crust worldwide (Fig. 11), are consistent with the adakitic rocks derived from a thickened lower crust and with the experimental melts of metabasaltic rocks at 1–4 GPa (Figs. 11c). In this case, we assert that the Azhang adakitic rocks were most likely generated by partial melting of a thickened lower crust that was still attached to the middle crust of the central Lhasa subterrane during the local lithospheric delamination, as recently suggested (Wang et al., 2014).

5.3. Nature of the thickened lower crust

Zircon Hf isotopic composition is generally accepted as an effective and sensitive tool for exploring the nature and evolution of lithospheric mantle and crustal basement (Griffin et al., 2002; Kemp et al., 2006; Zhu et al., 2011). Abundant zircon Hf isotope data of the Mesozoic magmatic rocks from the Lhasa terrane indicate that the southern and northern Lhasa subterranes have large positive $\varepsilon_{Hf}(t)$ values indicating the presence of a juvenile crust, while the central Lhasa subterrane has large negative $\varepsilon_{Hf}(t)$ values pointing to a micro-continent with ancient basement (Zhu et al., 2009a, 2011, and references therein).

The Azhang adakitic rocks were emplaced on the central Lhasa subterrane and thus are expected to inherit the isotopic characteristics of the ancient basement with large negative zircon $\varepsilon_{Hf}(t)$ values. However, the high positive $\varepsilon_{Hf}(t)$ values (up to +16.0) of the Azhang adakitic rocks are far away from those of the ancient central Lhasa basement-derived rocks (Fig. 4, Zhu et al., 2011, and reference therein). On the Pb–Pb diagram (Fig. 8b), the Azhang samples collectively define a linear array paralleling the modern MORB and distributed between the depleted MORB from the Bangong–Nujiang suture zone and Early Cretaceous arc-setting basalts (Zhu et al., 2006; Qiu et al., 2007). These isotopic characteristics suggest that the lower crust for producing the Azhang adakitic rocks beneath the central-northern Lhasa subterrane should be juvenile. The positive whole-rock $\varepsilon_{Nd}(t)$ (+2.5 to +5.6) of the Azhang adakitic rocks (Fig. 8a) confirms this suggestion.

Recent studies (Zhu et al., 2009a, 2011; Sui et al., 2013; Chen et al., 2014) show that mantle materials may have been enhanced in the central-northern Lhasa subterrane at ~113 Ma as indicated by the age vs. $\varepsilon_{Hf}(t)$ diagram (Fig. 4). Zhu et al. (2009a, 2011) interpret this phenomenon as a result of the slab break-off following the slab rollback of the southward subducted Bangong–Nujiang Ocean lithosphere that would facilitate the upwelling of asthenospheric materials and consequently basaltic magma underplating. Moreover, the youngest zircon Hf isotope crust model age (~130 Ma) of the Azhang adakitic rocks are similar to the emplacement timing of the Early Cretaceous subduction-related basalts in the northern Lhasa subterrane (110–130 Ma, Sui et al., 2013; Zhu et al., 2011). In this case, we suggest that the juvenile lower crust beneath the Azhang region was likely formed during the Early Cretaceous due to basaltic magma underplating in response to the slab rollback and break-off before and at ~113 Ma (Zhu et al., 2009a, 2011, Sui et al., 2013; Chen et al., 2014). Compared to these Early Cretaceous basalts in the northern Lhasa subterrane, the higher zircon $\varepsilon_{Hf}(t)$ values of the ~90 Ma Azhang adakitic rocks imply enhanced contributions from the mantle added to their source region. This behavior is consistent with the finding of Liu et al. (2014), who reported the presence of abundant zircon xenocrysts of ~90 Ma with positive zircon $\varepsilon_{Hf}(t)$ values from the Miocene ultrapotassic rocks in the central Lhasa subterrane. The small positive zircon $\varepsilon_{Hf}(t)$ value (as low as +8.9) and whole-rock $\varepsilon_{Nd}(t)$ value (as low as 2.5) may result from the limited involvement of materials from the central Lhasa basement with negative zircon $\varepsilon_{Hf}(t)$ values as documented by the Nyima Mg-rich volcanic rocks (Wang et al., 2014).

5.4. Tectonic implications

Our data reveal that the central Lhasa subterrane is likely characterized by the presence of a juvenile lower crust (at least locally) during the early Late Cretaceous, possibly caused by the slab rollback and

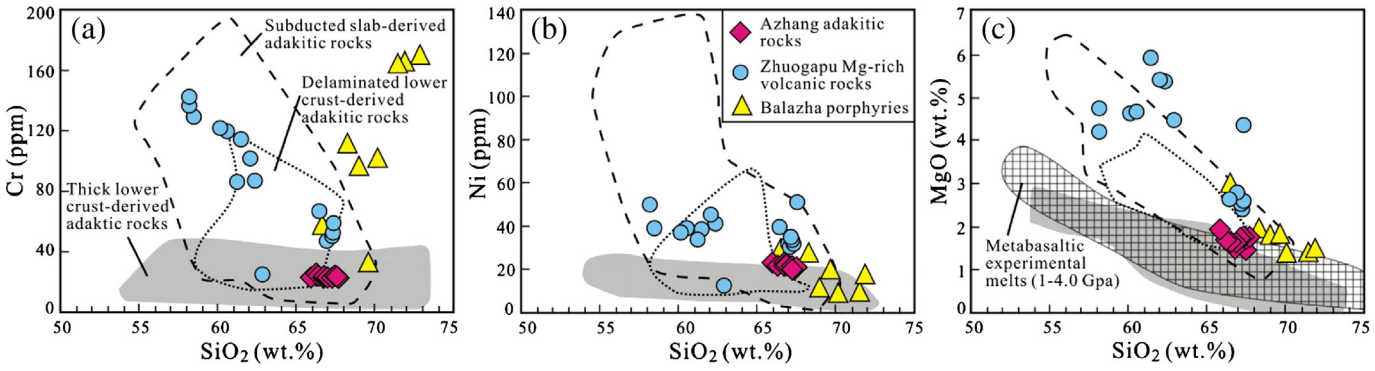

Fig. 11. Plots of Cr, Ni and MgO vs. SiO_2 for the Azhang adakitic rocks. The field of delaminated lower crust, subducted oceanic slab crust, and metabasaltic and eclogite experimental melts (1–4.0 GPa) follow the compilations of Wang et al. (2006a) and Huang et al. (2009); Balazha adakitic porphyries and Zhuogapu Mg-rich volcanic rocks are from Yu et al. (2011) and Wang et al. (2014).

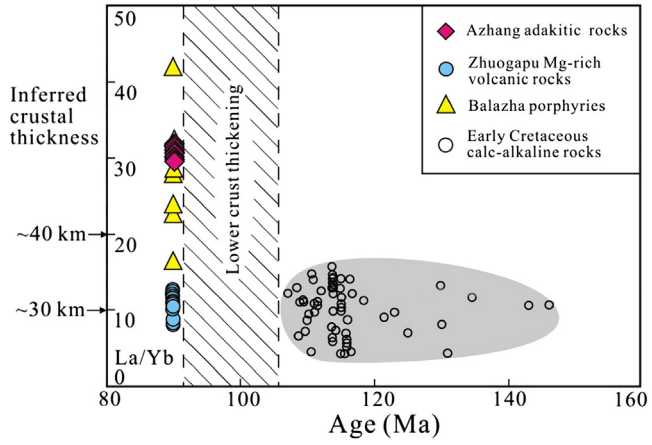

Fig. 12. Plots of La/Yb ratios vs. ages for the Azhang adakitic rocks and Early Cretaceous calc-alkaline rocks. The crustal thickness correlation is inferred after Chung et al. (2009). Date sources: Early Cretaceous calc-alkaline rocks are from Zhou et al. (2008); Zhu et al. (2009a, 2011) and references therein. Balazha adakitic porphyries and Zhuogapu Mg-rich volcanic rocks are from Yu et al. (2011) and Wang et al. (2014).

break-off of the southward Bangong–Nujiang ocean lithosphere in the Early Cretaceous (Zhu et al., 2009a; 2011; Sui et al., 2013; Chen et al., 2014). Experimental petrological studies indicate that partial melting of a lower mafic crust generally occurs at a depth of at least 40 km (Rapp et al., 1991, 2002, 2003), and the residual rutile phase always occurs at a depth of >50 km (pressure > 1.5 GPa, Xiong et al., 2005). Thus, the Azhang adakitic rocks can be interpreted as being generated under the crust at a depth of >50 km beneath the Lhasa terrane. The high Y and HREE abundances of the Early Cretaceous calc-alkaline rocks in the central-northern Lhasa subterrane indicate a normal crustal thickness (e.g., 30–35 km; Kay and Kay, 1993, 2002). On the diagram of La/Yb vs. age (Fig. 12), the crustal thickness was changed from ~30 km in the Early Cretaceous (~113 Ma) to ~50 km at ~90 Ma as indicated by the Azhang adakitic rocks. If this phenomenon is reasonable, a significant crustal thickening should have taken place within the central-northern Lhasa subterrane between the Early Cretaceous calc-alkaline rocks (~113 Ma) and the Azhang adakitic rocks (~90 Ma). This occurrence is supported by a recent study on the foreland basin deposits in Coqen, central Lhasa subterrane (Sun et al., in press), where the marine limestone (~113–96 Ma, Langshan Formation) was unconformably overlain by the continental molasses (~96–91 Ma, Jingzhushan/Daxiong Formation), indicating that the marine setting was transformed into a continental environment most likely between 96–91 Ma (Sun et al., in press). Coeval crustal shortening (ca. 125–95 Ma) has also been proposed in the Nyima basin, northern Lhasa subterrane (Kapp et al., 2007a; DeCelles et al., 2007).

The ongoing amalgamation between the Lhasa and Qiangtang terranes since the Early Cretaceous can readily account for the mechanism of crustal thickening. During the amalgamation, the buoyant lithospheric mantle beneath the Lhasa terrane had no more space to go, but leads to the extensive contraction and thickening along the Lhasa–Qiangtang collisional zone. This process could provide the driving force for the crustal shortening and thickening after the Lhasa–Qiangtang collision (Murphy et al., 1997; Kapp et al., 2007a, b; Volkmer et al., 2007). Due to this tectonic thickening, the lower portion of the thickened crust was transformed from the amphibolite facies to garnet-amphibolite facies, which would be the protolith for the ~90 Ma Azhang adakitic rocks. In addition to the tectonic thickening, the input of mantle-derived materials in response to the slab rollback and subsequent break-off generally exert significant effects on crustal thickening (Mo et al., 2007), which could provide additional effects for the crustal thickening of the central-northern Lhasa subterrane.

An important question is what triggered the heating up and melting of this thickened juvenile lower crust at ~90 Ma. In the central-northern Lhasa subterrane, magmatism was widely developed at ~90 Ma (Fig. 1b, Qu et al., 2006; Ma and Yue, 2010; Yu et al., 2011; Huang et al., 2013; Wang et al., 2014; Liu et al., 2014; Li et al., 2014). From a perspective of regional geology and geochemical signatures, Wang et al. (2014) proposed that the ~90 Ma Zhuogapu Mg-rich volcanic rocks from Nyima were generated by the delamination of lithosphere beneath the Lhasa–Qiangtang collision zone. Given the limited magmatism currently identified and the sedimentary records of the Coqen foreland basin (Sun et al., in press), we argue that the extent of this delamination was likely limited and restricted to the Lhasa–Qiangtang collision zone (Wang et al., 2014). In this case, the generation of the Azhang adakitic rocks can be described as follows.

Since the initial Lhasa–Qiangtang collision during the Late Jurassic–Early Cretaceous (Yin and Harrison, 2000; Kapp et al., 2005), the central-northern Lhasa subterrane has evolved into a continental interior setting. The central Lhasa subterrane would have an ancient basement in the lower crust (Zhu et al., 2009a, 2011). However, a possible

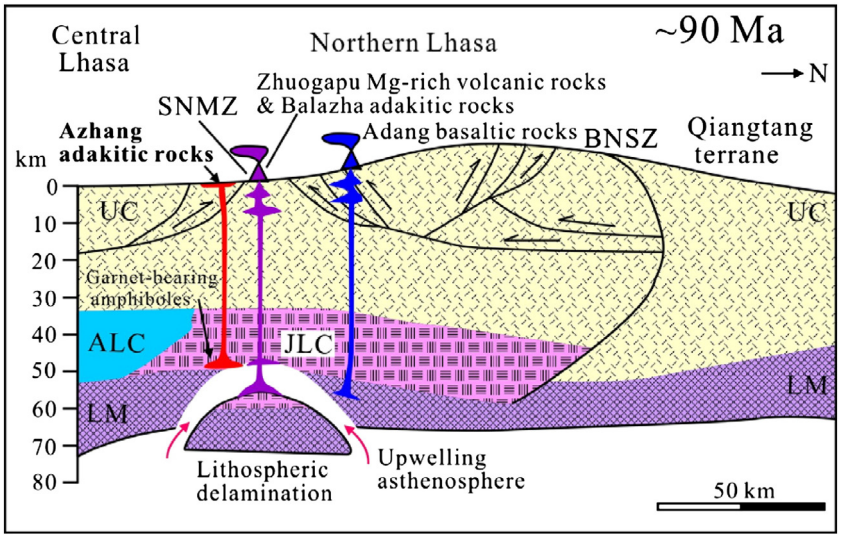

Fig. 13. Schematic illustrations showing the geodynamic evolution of the central-northern Lhasa subterrane at ~90 Ma. BNSZ = Bangong–Nujiang suture zone, SNMZ = Shiquan River–Nam Tso Mélange Zone, UC = Upper crust, ALC = Ancient lower crust, JLC = Juvenile lower crust, and LM = Lithospheric mantle.

model is that the break-off of the oceanic lithosphere in the Early Cretaceous triggered the partial melting of the upwelling asthenosphere (Zhu et al., 2009a; 2011). Such basaltic melts underplated and injected into the lower crust and could continue doing so for several million years after slab break-off, resulting in the formation of a juvenile lower crust. Due to tectonic shortening in response to the continuous Lhasa–Qiangtang amalgamation and magma underplating, the juvenile lower crust has experienced significant stacking and thickening. During this period, the lowermost part of the crust would have transformed from amphibolite facies to garnet-bearing amphibolite facies.

At ~90 Ma (Fig. 13), the partial melting of the lower portion of the thickened juvenile lower crust that is still attached to the middle crust is capable of producing the ~90 Ma Azhang adakitic melts as a result of lithospheric delamination in the Lhasa–Qiangtang collision zone (Wang et al., 2014). Thus, the emplacement of the Azhang adakitic rocks reported in this study and the coeval basaltic, Mg-rich volcanic, and adakitic rocks reported in recent studies (Ma and Yue, 2010; Yu et al., 2011; Wang et al., 2014) from the central-northern Lhasa subterrane likely represent different products of a common event (i.e., lithosphere delamination) in time and space beneath the Lhasa–Qiangtang collision zone.

6. Conclusions

(1) The Azhang volcanic rocks in the north edge of the central Lhasa subterrane were emplaced at ~90 Ma and show geochemical signatures similar to those of adakitic rocks.
(2) The Azhang adakitic rocks were most likely derived from partial melting of a thickened juvenile lower crust that would be formed by basaltic magma underplating in response to the slab rollback and break-off of the southward subducted Bangong–Nujiang Ocean lithosphere after the Lhasa–Qiangtang initial collision.
(3) The presence of the Azhang adakitic rocks indicates that the crust beneath the central-northern Lhasa subterrane has experienced thickening through tectonic shortening and basaltic magma underplating.

Acknowledgments

We sincerely thank Qian Liu, Bin Wu, Wei Pu, Gang Zeng, Huan-Ling Lei, Xiong Yan, and Zhong Han for their help in the labs. We thank Xiao-Lei Wang for his constructive suggestions and also Liang Liu, Xun Yu, Yan Xia and Lei Liu for their beneficial discussions. We are grateful to Prof. Sun-Lin Chung for his comments and editorial handling, and two anonymous reviewers for their constructive comments that improved this paper. This study was financially co-supported by the National Key Project for Basic Research of China (2012CB822001 and 2015CB452604), the Strategic Priority Research Program (B) of the Chinese Academy of Sciences (XDB03010301), and the Chinese National Natural Science Foundation (41472081, 41225006 and 41472061).

Appendix A. Descriptions of analytical methods

Zircon U–Pb dating and Hf isotopes

Zircons from the two samples (LS-P and LS-74) were separated using conventional magnetic and heavy-liquid separation methods. The single clean, morphologic zircon crystals were handpicked under a binocular microscope. The handpicked good quality zircons were mounted in epoxy resin and polished to expose the largest surface. Cathodoluminescence (CL) images were obtained for zircons to reveal any internal structures and inheritance.

Zircon U–Pb dating was conducted on a laser ablation inductively coupled plasma mass spectrometry (LA-ICP-MS) that is equipped with an Agilent 7500a ICP-MS connected to a New Wave Research 213 nm laser ablation system at the State Key Laboratory for Mineral Deposits Research (MiDeR), Nanjing University (NJU), China. More details for the instrumental conditions and analysis procedures are followed by Liu et al. (2013). The standard zircon was applied to correct the mass discrimination and elemental fractionation (Jackson et al., 2004). The primary Pb isotopic data were calculated and exported by GLITTER 4.4 software (van Achterbergh et al., 2001) and common Pb corrections were conducted following the program by Andersen (2002). The mean average ages and the concordia diagrams were obtained using the Isoplot/Ex program (version 2.49) of Ludwig (2001).

In situ zircon Hf isotopes were analyzed on the same zircon grains of U–Pb dating at MiDeR-NJU, China, using a Thermo Scientific Neptune (plus) MC-ICP-MS coupled to a New Wave 193 nm laser ablation system. The laser ablation beam is 50 μm in diameter and has an 8 Hz laser repetition rate and an energy of 10.91–11.05 J/cm^2. The data were collected 200 times in 1 min for each zircon grain. The standard Mud Tank zircon was analyzed every run to check the stability of the instrument. More detailed analytical conditions and procedures are referred to Wang et al. (2013). The calculation for the results was applied using 1.867×10^{-11} a^{-1} as the decay constant of ^{176}Lu (Soderlund et al., 2004). The results of $\varepsilon_{Hf}(t)$ and Hf crust model age (T^C_{DM}) are calculated using the methods by Bouvier et al. (2008) and Griffin et al. (2002)), respectively.

Whole-rock geochemical analysis

Based on petrographic observations, relatively fresh samples were selected for whole-rock geochemical analyses. Each sample was crushed to 200-mesh for further use. The analyses were also conducted at MiDeR-NJU, China.

Major elements were conducted on an X-ray fluorescence (XRF) spectrometer with an analysis precision of approximately ±1% for elements with concentrations >1.0 wt.%, and approximately ±10% for the elements with concentrations <1.0 wt.%. The trace element abundances were obtained by a Finnigan Element II ICP-MS following the procedures by Gao et al. (2003). The precision is commonly better than 5% and a few are better than 10%.

For whole-rock Sr–Nd–Pb isotopic analysis, 100 mg of 200-mesh powder was dissolved in the Teflon beakers with a mix of HF and HNO_3 acids. Sm–Nd and Rb–Sr were separated for isotopic analysis using AG50W × 8 resin and different eluent reagents. We used normal cation-exchange chromatography with an eluent of HCl to separate the REEs from the Rb–Sr system, while the Rb and Sr were separated and purified by a mixed eluent of pyridinium and DCTA complex. Sm and Nd isotopes were separated and purified with the eluent of HIBA by the cation-exchange resin (0.6 ml). The Sr and Nd isotopic concentrations were measured on a Finnigan Triton TI thermal ionization mass spectrometer (TIMS). Additional details about the conditions of instruments and analysis procedures follow those of Pu et al. (2004, 2005). The measured $^{87}Sr/^{86}Sr$ and $^{143}Nd/^{144}Nd$ ratios were normalized to $^{86}Sr/^{88}Sr = 0.1194$ and $^{146}Nd/^{144}Nd = 0.7219$, respectively, for the correction of instrumental fractionation. The measurements of the NIST SRM 987 Sr standard and JNdi-1 Nd standard were $^{87}Sr/^{86}Sr = 0.710259 \pm 0.000004$ (2σ) and $^{143}Nd/^{144}Nd = 0.512121 \pm 0.000003$ (2σ), respectively.

Another 100 mg of 200-mesh powder was dissolved into the Teflon beaker for whole-rock Pb isotopic measurements. Pb was separated and purified from the REEs using the conventional cation-exchange with the eluant of HBr. Pb isotopic ratios were analyzed on a Thermo Scientific Neptune Plus MC-ICP-MS. Repeated analysis of NIST 981 yielded the average ratios of $^{206}Pb/^{204}Pb$, $^{207}Pb/^{204}Pb$ and $^{208}Pb/^{204}Pb$ as 16.942 ± 4 (2σ), 15.498 ± 4 (2σ) and 36.728 ± 9 (2σ), with external precisions of less than 0.005, 0.005 and 0.0015, respectively.

Appendix B. LA-ICPMS U–Pb zircon age data

Table 1
LA-ICP-MS U–Pb results of zircons from samples LS-P and LS-74 of the Azhang adakitic rocks.

Analysis	Corrected ratios								Corrected ages (Ma)								Disc	Best	
Sample no.	$^{207}Pb/^{206}Pb$	1σ	$^{207}Pb/^{235}U$	1σ	$^{206}Pb/^{238}U$	1σ	$^{208}Pb/^{232}Th$	1σ	$^{207}Pb/^{206}Pb$	1σ	$^{207}Pb/^{235}U$	1σ	$^{206}Pb/^{238}U$	1σ	$^{208}Pb/^{232}Th$	1σ	(%)	ages	1σ
Sample LS74																			
LS-74-01	0.04747	0.00735	0.08926	0.01332	0.01364	0.00061	0.00219	0.0005	73	287	87	12	87	4	44	10	0	87	4
LS-74-02	0.0487	0.00274	0.09023	0.00496	0.01343	0.00028	0.00211	0.00016	133	127	88	5	86	2	43	3	2	86	2
LS-74-03	0.04739	0.00362	0.08782	0.00656	0.01344	0.00029	0.00381	0.00036	69	170	85	6	86	2	77	7	−1	86	2
LS-74-04	0.04642	0.00419	0.08689	0.0076	0.01358	0.00037	0.00408	0.00053	19	197	85	7	87	2	82	11	−2	87	2
LS-74-05	0.04972	0.00361	0.09258	0.00654	0.0135	0.00033	0.00146	0.00013	182	165	90	6	86	2	29	3	5	86	2
LS-74-06	0.04892	0.00896	0.08961	0.01565	0.01328	0.00076	0.00426	0.00149	144	339	87	15	85	5	86	30	2	85	5
LS-74-07	0.04783	0.00469	0.08897	0.00841	0.0135	0.0004	0.00388	0.00073	91	218	87	8	86	3	78	15	1	86	3
LS-74-08	0.04777	0.00492	0.08951	0.00884	0.01359	0.00046	0.00134	0.00026	88	227	87	8	87	3	27	5	0	87	3
LS-74-09	0.04747	0.00307	0.08801	0.00552	0.01345	0.00029	0.00339	0.00049	73	144	86	5	86	2	68	10	0	86	2
LS-74-10	0.04811	0.00305	0.08851	0.00544	0.01335	0.0003	0.00375	0.00062	105	142	86	5	85	2	76	12	1	85	2
LS-74-11	0.04993	0.00275	0.0945	0.00509	0.01373	0.00027	0.00379	0.00025	192	128	92	5	88	2	76	5	5	88	2
LS-74-12	0.04624	0.00399	0.0859	0.00718	0.01348	0.00036	0.00345	0.00037	10	190	84	7	86	2	70	7	−2	86	2
LS-74-13	0.04881	0.00378	0.09373	0.00706	0.01395	0.00034	0.00478	0.00055	139	175	91	7	89	2	96	11	2	89	2
LS-74-14	0.04785	0.00449	0.08983	0.00814	0.01362	0.0004	0.00287	0.00038	92	208	87	8	87	3	58	8	0	87	3
LS-74-15	0.04931	0.00241	0.09201	0.00439	0.01354	0.00026	0.00341	0.0003	163	113	89	4	87	2	69	6	2	87	2
LS-74-16	0.04772	0.00256	0.08762	0.00461	0.01333	0.00026	0.00333	0.00022	85	119	85	4	85	2	67	4	0	85	2
LS-74-17	0.04828	0.00258	0.08986	0.00468	0.01351	0.00026	0.00357	0.00034	113	121	87	4	87	2	72	7	0	87	2
LS-74-18	0.04883	0.00363	0.09347	0.00675	0.01389	0.00032	0.00364	0.00039	140	168	91	6	89	2	73	8	2	89	2
LS-74-19	0.04742	0.00297	0.089	0.00539	0.01361	0.00029	0.00439	0.00055	70	139	87	5	87	2	89	11	0	87	2
LS-74-20	0.05095	0.00331	0.09552	0.00599	0.01361	0.0003	0.00395	0.00052	239	150	93	6	87	2	80	10	7	87	2
LS-74-21	0.04615	0.00232	0.08828	0.00429	0.01388	0.00026	0.004	0.00056	5	108	86	4	89	2	81	11	−3	89	2
Sample LS-P																			
LS-P-01	0.04773	0.00286	0.0918	0.00545	0.01395	0.00026	0.00377	0.00026	86	133	89	5	89	2	76	5	0	89	2
LS-P-02	0.04804	0.00249	0.09216	0.00475	0.01392	0.00026	0.00287	0.00019	101	116	90	4	89	2	58	4	1	89	2
LS-P-03	0.04875	0.0071	0.09427	0.01336	0.01402	0.00053	0.0048	0.00084	136	292	91	12	90	3	97	17	1	90	3
LS-P-04	0.0479	0.00542	0.09265	0.01028	0.01403	0.00039	0.00356	0.00046	94	239	90	10	90	2	72	9	0	90	2
LS-P-05	0.04617	0.00515	0.09006	0.00986	0.01415	0.00039	0.0038	0.00047	7	225	88	9	91	2	77	9	−3	91	2
LS-P-06	0.04733	0.00265	0.09345	0.00518	0.01432	0.00026	0.00362	0.00029	66	124	91	5	92	2	73	6	−1	92	2
LS-P-07	0.04937	0.00463	0.09459	0.00864	0.01391	0.00041	0.00225	0.00029	165	213	92	8	89	3	45	6	3	89	3
LS-P-08	0.04726	0.00519	0.09164	0.00978	0.01406	0.00043	0.0038	0.00068	62	231	89	9	90	3	77	14	−1	90	3
LS-P-09	0.04499	0.00436	0.0849	0.00807	0.01368	0.00036	0.00355	0.0005	−20	192	83	8	88	2	72	10	−6	88	2
LS-P-10	0.04726	0.00383	0.08966	0.00718	0.01376	0.00029	0.00349	0.00036	62	181	87	7	88	2	70	7	−1	88	2
LS-P-11	0.04787	0.00308	0.09319	0.00593	0.01412	0.00028	0.00325	0.00033	93	144	90	6	90	2	66	7	0	90	2
LS-P-12	0.04739	0.00287	0.09134	0.00544	0.01397	0.00028	0.00372	0.00045	69	134	89	5	89	2	75	9	0	89	2
LS-P-13	0.05084	0.00278	0.09751	0.00526	0.01391	0.00026	0.00362	0.00029	234	127	94	5	89	2	73	6	6	89	2
LS-P-14	0.04663	0.00276	0.09015	0.00529	0.01402	0.00025	0.00367	0.00028	30	130	88	5	90	2	74	6	−2	90	2
LS-P-15	0.04795	0.00363	0.09343	0.00693	0.01412	0.00033	0.003	0.00033	97	170	91	6	90	2	61	7	1	90	2
LS-P-16	0.0478	0.00358	0.09272	0.00687	0.01407	0.00028	0.0032	0.00028	89	168	90	6	90	2	65	6	0	90	2
LS-P-17	0.04538	0.00506	0.08813	0.00964	0.0141	0.00041	0.00277	0.00033		218	86	9	90	3	56	7	−4	90	3
LS-P-18	0.05088	0.00477	0.09779	0.00901	0.01393	0.00035	0.00223	0.00023	235	214	95	8	89	2	45	5	7	89	2
LS-P-19	0.04511	0.00829	0.08826	0.01589	0.01419	0.0006	0.00196	0.00033	−14	304	86	15	91	4	40	7	−5	91	4
LS-P-20	0.0476	0.00773	0.09295	0.01473	0.01417	0.00055	0.00427	0.00096	79	298	90	14	91	3	86	19	−1	91	3
LS-P-21	0.04943	0.00378	0.09654	0.00725	0.01416	0.00033	0.0029	0.0003	168	174	94	7	91	2	59	6	3	91	2
LS-P-22	0.04624	0.0029	0.09047	0.00558	0.01417	0.00029	0.00273	0.0003	10	138	88	5	91	2	55	6	−3	91	2
LS-P-23	0.04727	0.00317	0.09153	0.006	0.01404	0.00031	0.00357	0.00057	63	149	89	6	90	2	72	11	−1	90	2
LS-P-24	0.04779	0.00504	0.0921	0.00944	0.01396	0.00044	0.00295	0.00071	89	230	89	9	89	3	60	14	0	89	3

Table 2
In situ zircon Hf isotopic data for samples LS-P and LS-74 of the Azhang adakitic rocks.

Sample no.	Age (Ma)	$^{176}Yb/^{177}Hf$	$^{176}Lu/^{177}Hf$	$^{176}Hf/^{177}Hf$	$\pm 2\sigma$	$(^{176}Hf/^{177}Hf)_t$	$\varepsilon_{Hf}(t)$	$T_{DM}/(Ga)$	$T^{C}_{DM}/(Ga)$
LS-74-01	87	0.013944	0.000438	0.283094	0.000029	0.283093	13.26	0.22	0.31
LS-74-02	86	0.014048	0.000487	0.282979	0.000039	0.282978	9.19	0.38	0.57
LS-74-03	86	0.016612	0.000635	0.282971	0.000045	0.282970	8.90	0.39	0.59
LS-74-04	87	0.014151	0.000513	0.283031	0.000044	0.283030	11.05	0.31	0.45
LS-74-05	86	0.022558	0.000871	0.283004	0.000033	0.283002	10.03	0.35	0.51
LS-74-06	85	0.019274	0.000610	0.283108	0.000040	0.283107	13.71	0.20	0.27
LS-74-07	86	0.019730	0.000661	0.283061	0.000024	0.283060	12.06	0.27	0.38
LS-74-08	87	0.023803	0.000810	0.283171	0.000049	0.283170	15.98	0.11	0.13
LS-74-09	86	0.016936	0.000585	0.283084	0.000022	0.283083	12.89	0.23	0.33
LS-74-10	85	0.025832	0.000899	0.283039	0.000032	0.283037	11.25	0.30	0.43
LS-74-11	88	0.013628	0.000463	0.283072	0.000025	0.283071	12.51	0.25	0.35
LS-74-12	86	0.012704	0.000447	0.283105	0.000026	0.283104	13.64	0.20	0.28
LS-74-13	89	0.016811	0.000665	0.283071	0.000022	0.283070	12.48	0.25	0.36
LS-74-14	87	0.021676	0.000722	0.283074	0.000031	0.283072	12.53	0.25	0.35
LS-74-15	87	0.040096	0.001281	0.283102	0.000029	0.283100	13.51	0.21	0.29
LS-74-16	85	0.019844	0.000688	0.283100	0.000031	0.283099	13.43	0.21	0.29
LS-74-17	87	0.026835	0.000917	0.283042	0.000032	0.283041	11.41	0.30	0.42
LS-74-18	89	0.019855	0.000691	0.283032	0.000032	0.283031	11.12	0.31	0.45
LS-74-19	87	0.028615	0.000957	0.283098	0.000028	0.283097	13.39	0.22	0.30
LS-74-20	87	0.030705	0.001047	0.283045	0.000032	0.283043	11.49	0.29	0.42
LS-74-21	89	0.024682	0.000836	0.283097	0.000029	0.283096	13.40	0.22	0.30
LS-P-01	89	0.017617	0.000647	0.283139	0.000023	0.283137	14.88	0.16	0.20
LS-P-02	89	0.019569	0.000680	0.283090	0.000026	0.283088	13.14	0.23	0.31
LS-P-03	90	0.021661	0.000747	0.283094	0.000026	0.283092	13.30	0.22	0.31
LS-P-04	90	0.013841	0.000520	0.283137	0.000022	0.283137	14.87	0.16	0.20
LS-P-05	91	0.014813	0.000528	0.283114	0.000021	0.283113	14.04	0.19	0.26
LS-P-06	92	0.020150	0.000713	0.283074	0.000034	0.283073	12.66	0.25	0.35
LS-P-07	89	0.024430	0.000824	0.283107	0.000028	0.283105	13.75	0.20	0.28
LS-P-08	90	0.024850	0.000876	0.283100	0.000024	0.283099	13.54	0.21	0.29
LS-P-09	88	0.018646	0.000671	0.283087	0.000023	0.283086	13.04	0.23	0.32
LS-P-10	88	0.016200	0.000566	0.283116	0.000025	0.283115	14.08	0.19	0.25
LS-P-11	90	0.014889	0.000542	0.283101	0.000020	0.283100	13.56	0.21	0.29
LS-P-12	89	0.014759	0.000521	0.283127	0.000024	0.283126	14.47	0.17	0.23
LS-P-13	89	0.023352	0.000822	0.283113	0.000034	0.283112	13.97	0.20	0.26
LS-P-14	90	0.020725	0.000737	0.283080	0.000031	0.283079	12.82	0.24	0.34
LS-P-15	90	0.018748	0.000655	0.283060	0.000027	0.283058	12.11	0.27	0.38
LS-P-16	90	0.014250	0.000501	0.283081	0.000025	0.283080	12.87	0.24	0.33
LS-P-17	90	0.021900	0.000726	0.283096	0.000031	0.283095	13.40	0.22	0.30
LS-P-18	89	0.017836	0.000618	0.283113	0.000023	0.283112	13.98	0.19	0.26
LS-P-19	91	0.021147	0.000734	0.283088	0.000032	0.283087	13.12	0.23	0.32
LS-P-20	91	0.016799	0.000572	0.283153	0.000025	0.283152	15.43	0.14	0.17
LS-P-21	91	0.018723	0.000646	0.283047	0.000023	0.283046	11.70	0.29	0.41
LS-P-22	91	0.028116	0.000950	0.283061	0.000024	0.283059	12.16	0.27	0.38
LS-P-23	90	0.020803	0.000737	0.283071	0.000021	0.283070	12.50	0.25	0.36
LS-P-24	89	0.027118	0.000888	0.283071	0.000023	0.283070	12.47	0.26	0.36

Table 3
Whole-rock major, trace element and Sr–Nd–Pb isotopic data of the Azhang adakitic rocks.

Sample	LS-74	LS-75	LS-H	LS-I	LS-J	LS-K	LS-N	LS-O	LS-P	LS-Q
Rock type	Dacite	Dacite	Dacite	Dacite	Dacite	Dacite	Dacite	Dacite	Dacite	Dacite
Major element (wt. %)										
SiO_2	63.48	64.18	65.06	64.16	66.04	63.30	64.38	63.89	64.57	65.36
TiO_2	0.38	0.39	0.40	0.39	0.41	0.38	0.37	0.38	0.37	0.40
Al_2O_3	16.67	16.56	16.63	16.54	17.15	16.42	16.75	16.61	16.76	17.14
Fe_2O_3	3.00	3.05	2.82	3.01	3.15	3.17	2.56	3.07	3.12	3.11
MnO	0.06	0.05	0.05	0.05	0.06	0.07	0.05	0.05	0.05	0.04
MgO	1.68	1.59	1.72	1.67	1.73	1.94	1.40	1.44	1.72	1.63
CaO	3.11	2.65	2.50	2.98	1.20	2.98	2.91	3.15	2.38	1.41
Na_2O	5.12	6.44	6.27	5.57	5.77	5.91	5.84	5.30	5.33	6.46
K_2O	2.09	1.13	1.26	1.94	1.88	1.66	1.15	1.55	1.46	1.09
P_2O_5	0.23	0.21	0.20	0.20	0.21	0.19	0.19	0.20	0.20	0.21
LOI	3.79	3.40	3.42	3.67	2.55	3.57	3.74	3.96	3.50	2.57
TOTAL	99.60	99.65	100.32	100.17	100.16	99.58	99.34	99.61	99.45	99.42
$Mg^{\#}$	56	58	56	55	58	55	51	55	54	54
Trace element (ppm)										
Li	31.5	33.0	32.2	25.4	29.4	32.3	24.9	24.5	26.9	27.4
Be	0.96	0.88	0.92	0.91	0.95	0.96	0.87	0.94	0.81	0.81
Sc	7.84	7.24	6.73	7.44	7.68	7.61	7.52	7.34	7.34	7.15
V	80.3	87.0	75.3	78.8	79.4	80.9	76.3	76.8	78.4	82.9
Cr	26.8	29.6	22.9	23.5	23.8	23.8	21.9	23.2	23.1	25.2
Co	8.86	7.67	8.10	8.47	8.63	9.59	7.06	7.70	8.47	8.23

Table 3 (*continued*)

Sample	LS-74	LS-75	LS-H	LS-I	LS-J	LS-K	LS-N	LS-O	LS-P	LS-Q
Rock type	Dacite	Dacite	Dacite	Dacite	Dacite	Dacite	Dacite	Dacite	Dacite	Dacite
Ni	23.9	24.9	22.2	22.1	21.9	23.9	18.9	20.7	22.5	22.5
Cu	33.5	70.5	74.0	42.1	50.2	69.9	102.7	46.7	56.8	55.7
Zn	47.7	46.9	46.8	48.7	48.8	48.8	50.9	50.2	54.0	44.8
Ga	18.7	18.9	17.8	18.3	18.8	18.4	18.9	18.3	19.8	19.6
Rb	33.9	32.0	29.3	31.6	30.8	33.4	31.6	30.7	32.5	30.2
Sr	761	836	703	655	626	796	668	737	554	635
Y	8.63	8.35	7.98	8.43	8.96	8.54	8.09	7.96	8.45	7.96
Zr	117	113	108	110	113	114	111	111	115	116
Nb	9.43	9.19	8.85	9.00	9.07	8.95	9.00	9.03	9.18	9.22
Sn	0.48	0.51	0.52	0.54	0.50	0.51	0.51	0.53	0.53	0.54
Cs	4.96	4.36	2.84	5.19	5.10	3.59	3.08	7.38	6.41	4.82
Ba	385	228	233	511	269	1290	177	237	200	144
La	27.2	26.7	26.6	28.3	28.5	26.6	26.2	26.3	27.7	27.5
Ce	51.2	50.2	47.8	52.2	51.2	51.3	49.9	50.0	51.8	53.3
Pr	6.41	6.21	5.98	6.59	6.68	6.24	6.18	6.20	6.48	6.38
Nd	24.2	23.4	22.6	24.7	25.6	23.4	23.3	23.2	24.6	24.0
Sm	3.78	3.53	3.51	3.77	3.95	3.63	3.62	3.58	3.84	3.74
Eu	1.09	1.03	0.98	1.12	1.10	1.31	0.98	0.99	1.04	0.87
Gd	2.98	2.79	2.75	2.98	3.11	2.87	2.76	2.81	2.99	2.89
Tb	0.38	0.37	0.35	0.37	0.39	0.37	0.35	0.35	0.38	0.36
Dy	1.75	1.72	1.65	1.75	1.83	1.71	1.63	1.66	1.77	1.67
Ho	0.32	0.31	0.30	0.31	0.33	0.31	0.29	0.30	0.32	0.30
Er	0.89	0.87	0.82	0.87	0.90	0.86	0.82	0.82	0.89	0.85
Tm	0.15	0.15	0.14	0.14	0.15	0.15	0.14	0.14	0.15	0.15
Yb	0.92	0.91	0.86	0.90	0.93	0.90	0.87	0.87	0.94	0.92
Lu	0.13	0.13	0.13	0.13	0.13	0.13	0.13	0.13	0.14	0.13
Hf	3.30	3.19	3.08	3.17	3.29	3.23	3.07	3.16	3.30	3.30
Ta	0.37	0.37	0.36	0.36	0.37	0.36	0.35	0.36	0.37	0.37
Pb	12.25	6.60	22.23	9.80	8.16	12.34	12.85	7.66	3.14	3.27
Th	5.49	5.45	5.31	5.55	5.51	5.42	5.31	5.27	5.67	5.71
U	1.49	1.65	1.50	1.43	1.49	1.66	1.64	1.45	1.69	1.62
Sr-Nd-Pb isotopic compositions										
$^{87}Rb/^{86}Sr$	0.1290	0.1107	0.1206		0.1422	0.1214	0.1369	0.1204	0.1694	0.1376
$^{87}Sr/^{86}Sr$	0.7054	0.7062	0.7055		0.7054	0.7056	0.7061	0.7059	0.7060	0.7061
2σ	0.000007	0.000003	0.000007		0.000006	0.000005	0.000006	0.000008	0.000007	0.000006
$(^{87}Sr/^{86}Sr)_t$	0.7052	0.7060	0.7054		0.7053	0.7055	0.7060	0.7057	0.7058	0.7059
$^{147}Sm/^{144}Nd$	0.0944	0.0910	0.0939		0.0933	0.0935	0.0940	0.0934	0.0942	0.0940
$^{143}Nd/^{144}Nd$	0.5128	0.5128	0.5128		0.5128	0.5127	0.5129	0.5128	0.5128	0.5128
2σ	0.000010	0.000018	0.000009		0.000020	0.000042	0.000019	0.000026	0.000002	0.000030
$\varepsilon_{Nd}(t)$	3.6	4.3	4.4		4.3	2.5	5.6	4.3	4.4	4.2
$(^{143}Nd/^{144}Nd)_t$	0.5127	0.5127	0.5127		0.5127	0.5127	0.5128	0.5127	0.5127	0.5127
T_{DM}^{c}/Ga	0.60	0.54	0.53		0.54	0.69	0.44	0.55	0.54	0.55
$^{206}Pb/^{204}Pb$	18.62	18.78	18.56		18.68	18.58	18.64	18.65	18.90	18.77
2σ	0.0029	0.0035	0.0013		0.0019	0.0022	0.0047	0.0014	0.0049	0.0037
$^{207}Pb/^{204}Pb$	15.58	15.59	15.58		15.59	15.58	15.60	15.60	15.61	15.60
2σ	0.0026	0.0030	0.0011		0.0017	0.0019	0.0040	0.0011	0.0042	0.0030
$^{208}Pb/^{204}Pb$	38.69	38.85	38.63		38.78	38.65	38.77	38.74	39.01	38.94
2σ	0.0061	0.0071	0.0027		0.0040	0.0048	0.0102	0.0032	0.0103	0.0077

References

Allègre, C.J., Minster, J.F., 1978. Quantitative models of trace element behavior in magmatic processes. Earth and Planetary Science Letters 38, 1–25.

Andersen, T., 2002. Correction of common lead in U/Pb analyses that do not report ^{204}Pb. Chemical Geology 192, 59–79.

Atherton, M.P., Petford, N., 1993. Generation of sodium-rich magmas from newly underplated basaltic crust. Nature 362, 144–146.

Bizzarro, M., Baker, J., Ulfbeck, D., 2003. A new digestion and chemical separation technique for rapid and highly reproducible determination of Lu/Hf and Hf isotope ratios in geological materials by MC-ICP-MS. Geostandards and Geoanalytical Research 27, 133–145.

Bouvier, A., Vervoort, J.D., Patchett, P.J., 2008. The Lu–Hf and Sm-Nd isotopic composition of CHUR: constraints from unequilibrated chondrites and implications for the bulk composition of terrestrial planets. Earth and Planetary Science Letters 273, 48–57.

Castillo, P.R., 2006. An overview of adakite petrogenesis. Chinese Science Bulletin 51, 257–268. http://dx.doi.org/10.1007/s11434-006-0257-7.

Castillo, P.R., 2012. Adakite petrogenesis. Lithos 134–135, 304–316.

Castillo, P.R., Janney, P.E., Solidum, R.U., 1999. Petrology and geochemistry of Camiguin island, southern Philippines: insights to the source of adakites and other lavas in a complex arc setting. Contributions to Mineralogy and Petrology 134, 33–51.

Chen, Y., Zhu, D.C., Zhao, Z.D., Meng, F.Y., Wang, Q., Santosh, M., Wang, L.Q., Dong, G.C., Mo, X.X., 2014. Slab breakoff triggered ca. 113 Ma magmatism around Xainza area of the Lhasa Terrane, Tibet. Gondwana Research 26, 449–463.

Chu, M.F., Chung, S.L., Song, B.A., Liu, D.Y., O'Reilly, S.Y., Pearson, N.J., Ji, J.Q., Wen, D.J., 2006. Zircon U–Pb and Hf isotope constraints on the Mesozoic Tectonics and crustal evolution of southern Tibet. Geology 34, 745–748.

Chung, S.L., Chu, M.F., Zhang, Y., Xie, Y., Lo, C.H., Lee, T.Y., Lan, C.Y., Li, X.H., Zhang, Q., Wang, Y., 2005. Tibetan tectonic evolution inferred from spatial and temporal variations in post-collisional magmatism. Earth-Science Reviews 68, 173–196.

Chung, S.L., Chu, M.F., Ji, J.Q., O'Reilly, S.Y., Pearson, N.Y., Liu, D.Y., Lee, T.Y., Lo, C.H., 2009. The nature and timing of crustal thickening in Southern Tibet: geochemical and zircon Hf isotopic constraints from postcollisional adakites. Tectonophysics 477, 36–48.

DeCelles, P.G., Kapp, P., Ding, L., Gehrels, G.E., 2007. Late Cretaceous to mid-Tertiary basin evolution in the central Tibetan Plateau: changing environments in response to tectonic partitioning, aridification, and regional elevation gain. Geological Society of America Bulletin 119, 654–680.

Defant, M.J., Drummond, M.S., 1990. Derivation of some modern arc magmas by melting of young subducted lithosphere. Nature 347, 662–665.

Ding, L., Lai, Q.Z., 2003. New geological evidence of crustal thickening in the Gangdese block prior to the Indo-Asian collision. Chinese Science Bulletin 48, 1604–1610.

Ding, L., Kapp, P., Zhong, D., Deng, W., 2003. Cenozoic volcanism in Tibet: evidence for a transition from Oceanic to continental subduction. Journal of Petrology 44, 1833–1865.
Drummond, M.S., Defant, M.J., 1990. A model for trondhjemite–tonalite–dacite genesis and crustal growth via slab melting: Archaean to modern comparisons. Journal of Geophysical Research 95, 21503–21521.
Gao, J.F., Lu, J.J., Lin, Y.P., Pu, W., 2003. Analysis of trace elements in rock samples using HR-ICPMS. Journal of Nanjing University (Natural Sciences) 39, 844–850 (in Chinese with English abstract).
Griffin, W.L., Wang, X., Jackson, S.E., Pearson, N.J., O'Reilly, S.Y., Xu, X.S., Zhou, X.M., 2002. Zircon chemistry and magma mixing, SE China: in-situ analysis of Hf isotopes, Tonglu and Pingtan igneous complexes. Lithos 61, 237–269.
Harris, N.B.W., Inger, S., Xu, R., 1990. Cretaceous plutonism in Central Tibet: an example of post-collision magmatism? Journal of Volcanology and Geothermal Research 44, 21–32.
Harrison, T.M., Grove, M., McKeegan, K.D., Coath, C.D., Lovera, O.M., Fort, P.L., 1999. Origin and episodic emplacement of the Manaslu Intrusive Complex, Central Himalaya. Journal of Petrology 40, 3–19.
Hastie, A.R., Kerr, A.C., Pearce, J.A., Mitchell, S.F., 2007. Classification of altered volcanic island arc rocks using immobile trace elements: development of the Th–Co discrimination diagram. Journal of Petrology 48, 2341–2357.
Hoskin, P.W.O., Schaltegger, U., 2003. The composition of zircon and igneous and metamorphic petrogenesis. Reviews in Mineralogy and Geochemistry 53, 27–55.
Hou, Z.Q., Guo, Y.F., Qu, X.M., Rui, Z.Y., Mo, X.X., 2004. Origin of adakitic intrusives generated during mid-Miocene east–west extension in southern Tibet. Earth and Planetary Science Letters 220, 139–155.
Huang, X.L., Xu, Y.G., Lan, J.B., Yang, Q.J., Luo, Z.Y., 2009. Neoproterozoic adakitic rocks from Mopanshan in the western Yangtze Craton: partial melts of a thickened lower crust. Lithos 112, 367–381.
Huang, H.X., Li, G.M., Chen, H.A., Shi, H.Z., Liu, B., Zhu, X.P., Zeng, Q.G., Li, Z., 2013. Molybdenite Re–Os isotope age and metallogenic significance of Sebuta copper molybdenum deposit in Tibet. Acta Geologica Sinica 87, 240–244 (in Chinese with English abstract).
Jackson, S.E., Pearson, N.J., Griffin, W.L., Belousoval, E.A., 2004. The application of laser ablation-inductively coupled plasma-mass spectrometry (LA-ICP-MS) to in situ U/Pb zircon geochronology. Chemical Geology 211, 47–69.
Ji, W.Q., Wu, F.Y., Chung, S.L., Li, J.X., Liu, C.Z., 2009. Zircon U–Pb geochronology and Hf isotopic constraints on petrogenesis of the Gangdese Batholith, Southern Tibet. Chemical Geology 262, 229–245.
Kapp, P., Yin, A., Harrison, T.M., Ding, L., 2005. Cretaceous–Tertiary shortening, basin development, and volcanism in central Tibet. Geological Society of America Bulletin 117, 865–878.
Kapp, P., Decelles, P.G., Gehrels, G.E., Heizler, M., Ding, L., 2007a. Geological records of the Lhasa-Qiangtang and Indo-Asian collisions in the Nima area of Central Tibet. Geological Society of America Bulletin 119, 917–932.
Kapp, P., DeCelles, P.G., Leier, A.L., Fabijanic, J.M., He, S., Pullen, A., Gehrels, G.E., 2007b. The Gangdese retroarc thrust belt revealed. GSA Today. 17 p. 7. http://dx.doi.org/10.1130/GSAT01707A.1.
Kay, R.W., Kay, S.M., 1993. Delamination and delamination magmatism. Tectonophysics 217, 177–189.
Kay, R.W., Kay, S.M., 2002. Andean adakites: three ways to make them. Acta Petrologica Sinica 18, 303–311.
Kay, S.M., Ramos, V.A., Marquez, M., 1993. Evidence in Cerro Pampa volcanic rocks of slab melting prior to ridge trench collision in southern South America. The Journal of Geology 101, 703–714.
Kemp, A.I.S., Hawkesworth, C.J., Paterson, B.A., Kinny, P.D., 2006. Episodic growth of the Gondwana supercontinent from hafnium and oxygen isotopes in zircon. Nature 439, 580–583.
Lai, S.C., Qin, J.F., Grapes, R., 2008. Petrology and geochemistry of the granulite xenoliths from Cenozoic Qiangtang volcanic field: implication for the nature of the lower crust in the northern Tibetan plateau and the genesis of Cenozoic volcanic rocks. Acta Petrologica Sinica 24, 325–336 (in Chinese with English abstract).
Leeder, M.R., Smith, A.B., Jixiang, Y., 1988. Sedimentology and palaeoenvironmental evolution of the 1985 Lhasa to Golmud Geotraverse. Philosophical Transactions of the Royal Society of London, Series A 327, 107–143.
Li, Y.L., He, J., Wang, C.S., Santosh, M., Dai, J.G., Zhang, Y.X., Wei, Y.S., Wang, J.G., 2013. Late Cretaceous K-rich magmatism in central Tibet: evidence for early elevation of the Tibetan plateau? Lithos 160–161, 1–13.
Li, H.L., Yang, S., Li, D.W., Zhang, S., Lv, Z.W., Chen, G.F., 2014. Geochronology, geochemistry, tectonic setting and metallogenetic significance of the Late Cretaceous quartz monzonite in the Northwestern Gangdise Terrane. Geotectonica et Metallogenia 38, 694–705 (in Chinese with English abstract).
Liu, D.Z., Tao, X.F., Ma, R.Z., Shi, H., Zhu, L.D., Hu, X. W., 2004. 1: 250, 000 geological report of Coqen County with geological map. Chengdu University of Technology, Chengdu, 163-183 (in Chinese with English abstract).
Liu, L., Qiu, J.S., Li, Z., 2013. Origin of mafic microgranular enclaves (MMEs) and their host quartz monzonites from the Muchen pluton in Zhejiang Province, Southeast China: implications for magma mixing and crust–mantle interaction. Lithos 160–161, 145–163.
Liu, D., Zhao, Z.D., Zhu, D.C., Niu, Y.L., Harrison, T.M., 2014. Zircon xenocrysts in Tibetan ultrapotassic magmas: imaging the deep crust through time. Geology 42, 43–46.
Ludwig, K.R., 2001. Isoplot/Ex (rev. 2.49): a geochronological toolkit for Microsoft Excel. Special Publication 1. Berkeley Geochronology Center, pp. 1–58.
Ma, G.L., Yue, Y.H., 2010. Cretaceous volcanic rocks in northern Lhasa Block: constraints on the tectonic evolution of Gangdise Arc. Acta Petrologica Et Mineralogica 29, 525–538 (in Chinese with English abstract).
Ma, L., Wang, Q., Li, Z.X., Wyman, D.A., Jiang, Z.Q., Yang, J.H., Gou, G.N., Guo, H.F., 2013a. The early Late Cretaceous (ca. 93 Ma) norites and hornblendites in the Milin area, eastern Gangdese: lithosphere–asthenosphere interaction during slab roll-back and an insight into early Late Cretaceous (ca. 100–80 Ma) magmatic "flare-up" in southern Lhasa (Tibet). Lithos 172–173, 17–30.
Ma, L., Wang, Q., Wyman, D.A., Jiang, Z.Q., Yang, J.H., Li, Q.L., Gou, G.N., Guo, H.F., 2013b. Late Cretaceous crustal growth in the Gangdese area, southern Tibet: petrological and Sr–Nd–Hf–O isotopic evidence from Zhengga diorite–gabbro. Chemical Geology 349–350, 54–70.
Ma, L., Wang, Q., Wyman, D.A., Li, Z.X., Jiang, Z.Q., Yang, J.H., 2013c. Late Cretaceous (100–89 Ma) magnesian charnockites with adakitic affinities in the Milin area, eastern Gangdese: partial melting of subducted oceanic crust and implications for crustal growth in southern Tibet. Lithos 175–176, 315–332.
Martin, H., 1999. The adakitic magmas: modern analogues of Archaean granitoids. Lithos 46, 411–429.
Martin, H., Smithies, R.H., Rapp, R., Moyen, J.F., Champion, D., 2005. An overview of adakite, tonalite–trondhjemite–granodiorite (TTG), and sanukitoid: relationships and some implications for crustal evolution. Lithos 79, 1–24.
Miller, C., Schuster, R., Klotzli, U., Frank, W., Purtscher, F., 1999. Post-collisional potassic and ultrapotassic magmatism in SW Tibet: geochemical and Sr–Nd–Pb–O isotopic constraints for mantle source characteristics and petrogenesis. Journal of Petrology 40, 1399–1424.
Mo, X.X., Dong, G.C., Zhao, Z.D., Zhou, S., Wang, L.L., Qiu, R.Z., Zhang, F.Q., 2005. Spatial and temporal distribution and characteristics of Granitoids in the Gangdese, Tibet and implication for crustal growth and evolution. Geological Journal of China Universities 11, 281–290 (in Chinese with English abstract).
Mo, X.X., Hou, Z.Q., Niu, Y.L., Dong, G.C., Qu, X.M., Zhao, Z.D., Yang, Z.M., 2007. Mantle contributions to crustal thickening during continental collision: evidence from Cenozoic igneous rocks in southern Tibet. Lithos 96, 225–242.
Mo, X.X., Niu, Y.L., Dong, G.C., Zhao, Z.D., Hou, Z.Q., Zhou, S., Ke, S., 2008. Contribution of syncollisional felsic magmatism to continental crust growth: a case study of the Paleogene Linzizong volcanic Succession in southern Tibet. Chemical Geology 250, 49–68.
Murphy, M.A., Yin, A., Harrison, T.M., Dürr, S.B., Chen, Z., Ryerson, F.J., Kidd, W.S.F., Wang, X., Zhou, X., 1997. Did the Indo-Asian collision alone create the Tibetan plateau? Geology 25, 719–722.
Pan, Y., 1993. Unroofing History and Structural Evolution of the Southern Lhasa Terrane, Tibetan Plateau: Implications for the Continental Collision Between India and Asia. (Ph.D. thesis), State University of New York, Albany (287 pp.).
Pan, G.T., Ding, J., Yao, D.S., Wang, L.Q., 2004. Guidebook of 1:1500000 Geologic Map of the Qinghai-Xizang (Tibet) Plateau and Adjacent Areas, China. Chengdu Cartographic Publishing House, Chengdu pp, 1-48 (in Chinese).
Pan, G.T., Mo, X.X., Hou, Z.Q., Zhu, D.C., Wang, L.Q., Li, G.M., Zhao, Z.D., Geng, Q.R., Liao, Z.L., 2006. Spatial–temporal framework of the Gangdese Orogenic Belt and its evolution. Acta Petrologica Sinica 22, 521–533 (in Chinese with English abstract).
Pan, G.T., Wang, L.Q., Li, R.S., Yuan, S.H., Ji, W.H., Yin, F.G., Zhang, W.P., Wang, B.D., 2012. Tectonic evolution of the Qinghai–Tibet Plateau. Journal of Asian Earth Sciences 53, 3–14.
Parrish, R.R., Hodges, K.V., 1996. Isotopic constraints on the age and provenance of the Lesser and Greater Himalayan sequences, Nepalese Himalaya. Geological Society of American Bulletin 108, 904–911.
Petford, N., Atherton, M., 1996. Na-rich partial melts from newly underplated basaltic crust: the Cordillera Blanca batholith, Peru. Journal of Petrology 37, 1491–1521.
Pu, W., Zhao, K.D., Ling, H.F., Jiang, S.Y., 2004. High precision Nd isotope measurement by Triton TI Mass Spectrometry. Acta Geoscientica Sinica 25, 271–274 (in Chinese with English abstract).
Pu, W., Gao, J.F., Zhao, K.D., Lin, H.F., Jiang, S.Y., 2005. Separation methodof Rb/Sr, Sm/Nd using DCTA and HIBA. Journal of Nanjing University (Natural Sciences) 41, 445–450 (in Chinese with English abstract).
Pullen, A., Kapp, P., Gehrels, G., DeCelles, P., Brown, E., Fabijanic, M., Ding, L., 2008. Gangdese retroarc thrust belt and foreland basin deposits in the Damxung area, southern Tibet. Journal of Asian Earth Sciences 33, 323–336.
Qiu, R.Z., 2002. Igneous Rocks and Tectonic Evolution of the Neo-Tethyan in the Western Tibetan Plateau. Unpublished Ph.D. thesis submitted to the China University of Geosciences, Beijing (in Chinese with English abstract).
Qiu, R.Z., Zhou, S., Li, T.D., Deng, J.F., Xiao, Q.H., Wu, Z.X., Cai, Z.Y., 2007. The tectonic-setting of ophiolites in the western Qinghai–Tibet Plateau, China. Journal of Asian Earth Sciences 29, 215–228.
Qu, X.M., Xin, H.B., Wu, W.Y., Yang, Z.S., Li, Z.Q., 2006. Discovery and significance of copper-bearing bimodal rock series in Coqin area of Tibet. Acta Petrologica Sinica 22, 707–716 (in Chinese with English abstract).
Rapp, R.P., Watson, E.B., Miller, C.F., 1991. Partial melting of amphibolite, eclogite and the origin of Archaean trondhjemites and tonalites. Precambrian Research 51, 1–25.
Rapp, R.P., Xiao, L., Shimizu, N., 2002. Experimental constraints on the origin of potassium-rich adakite in east China. Acta Petrologica Sinica 18, 293–311.
Rapp, R.P., Shimizu, N., Norman, M.D., 2003. Growth of early continental crust by partial melting of eclogite. Nature 425, 605–609.
Richards, J.P., Kerrich, R., 2007. Adakite-like rocks: their diverse origins and questionable role in metallogenesis. Economic Geology 102, 537–576.
Scott, R., Wan, X., Sha, J., Wen, S., 2010. Rudists of Tibet and the Tarim basin, China: significance to requieniidae phylogeny. Journal of Paleontology 84, 444–465.
Soderlund, U., Patchett, P.J., Vervoort, J.D., Isachsen, C.E., 2004. The ^{176}Lu decay constant determined by Lu–Hf and U–Pb isotope systematics of Precambrian mafic intrusions. Earth and Planetary Science Letters 219, 311–324.
Sui, Q.L., Wang, Q., Zhu, D.C., Zhao, Z.D., Chen, Y., Santosh, M., Hu, Z.C., Yuan, H.L., Mo, X.X., 2013. Compositional diversity of ca. 110 Ma magmatism in the northern Lhasa Terrane, Tibet: implications for the magmatic origin and crustal growth in a continent–continent collision zone. Lithos 168–169, 144–159.
Sun, S.S., McDonough, W.F., 1989. Chemical and isotope systematics of oceanic basalts: implications for mantle composition and processes. In: Saunders, A.D. (Ed.), Magmatism in Ocean Basins. Geological Society Publication 42, pp. 313–345.

Sun, G.Y., Hu, X.M., Sinclair, H.D., Marcelle, B.D., Wang, J.G., 2015. Late Cretaceous evolution of the Coqen basin (Lhasa terrane) and implications for early topographic growth on the Tibetan Plateau. Geological Society of America Bulletin http://dx.doi.org/10.1130/B31137.1 (in press).

Topuz, G., Altherr, R., Schwarz, W.H., Siebel, W., Satır, M., Dokuz, A., 2005. Post-collisional plutonism with adakite-like signatures: the Eocene Saraycık granodiorite (Eastern Pontides, Turkey). Contributions to Mineralogy and Petrology 150, 441–455.

van Achterbergh, E., Ryan, C.G., Jackson, S.E., Griffin, W.L., 2001. Data reduction software for LA-ICP-MS: appendix. In: Sylvester, P.J. (Ed.), Laser Ablation-ICP-Mass Spectrometry in the Earth Sciences: Principles and Applications. 29. Mineralogical Association of Canada (MAC) Short Course Series, Ottawa, Ontario, Canada, pp. 239–243.

Volkmer, J.E., Kapp, P., Guynn, J.H., Lai, Q., 2007. Cretaceous–Tertiary structural evolution of the north central Lhasa terrane, Tibet. Tectonics 26, TC6007. http://dx.doi.org/10.1029/2005TC001832.

Wang, Q., Xu, J.F., Zhao, Z.H., Bao, Z.W., Xu, W., Xiong, X.L., 2004a. Cretaceous high-potassium intrusive rocks in the Yueshan–Hongzhen area of east China: adakites in an extensional tectonic regime within a continent. Geochemical Journal 38, 417–434.

Wang, Q., Zhao, Z.H., Bao, Z.W., Xu, J.F., Liu, W., Li, C.F., Bai, Z.H., Xiong, X.L., 2004b. Geochemistry and petrogenesis of the Tongshankou and Yinzu adakitic intrusive rocks and the associated porphyry copper–molybdenum mineralization in southeast Hubei, east China. Resource Geology 54, 137–152.

Wang, Q., McDermott, F., Xu, J.F., Bellon, H., Zhu, Y.T., 2005. Cenozoic K-rich adakitic volcanic rocks in the Hohxil area, northern Tibet: lower crustal melting in an intracontinental setting. Geology 33, 465–468.

Wang, Q., Xu, J.F., Jian, P., Bao, Z.W., Zhao, Z.H., Li, C.F., Xiong, X.L., Ma, J.L., 2006a. Petrogenesis of adakitic porphyries in an extensional tectonic setting, Dexing, South China: implications for the genesis of porphyry copper mineralization. Journal of Petrology 47, 119–144.

Wang, Q., Wyman, D.A., Xu, J.F., Zhao, Z.H., Jian, P., Xiong, X.L., Bao, Z.W., Li, C.F., Bai, Z.H., 2006b. Petrogenesis of Cretaceous adakitic and shoshonitic igneous rocks in the Luzong area, Anhui Province (eastern China): implications for geodynamics and Cu–Au mineralization. Lithos 89, 424–446.

Wang, X.L., Zhou, J.C., Wan, Y.S., Kitajima, K., Wang, D., Bonamici, C., Qiu, J.S., Sun, T., 2013. Magmatic evolution and crustal recycling for Neoproterozoic strongly peraluminous granitoids from southern China: Hf and O isotopes in zircon. Earth and Planetary Science Letters 366, 71–82.

Wang, Q., Zhu, D.C., Zhao, Z.D., Liu, S.A., Chung, S.L., Li, S.M., Liu, D., Dai, J.G., Wang, L.Q., Mo, X.X., 2014. Origin of the ca. 90 Ma magnesia-rich volcanic rocks in SE Nyima, central Tibet: products of lithospheric delamination underneath the Lhasa–Qiangtang collision zone. Lithos 198–199, 24–37.

Wen, D.R., Chung, S.L., Song, B., Lizuka, Y., Yang, H.J., Ji, J.Q., Liu, D.Y., Gallet, S., 2008. Late Cretaceous Gangdese intrusions of adakitic geochemical characteristics, SE Tibet: petrogenesis and tectonic implications. Lithos 105, 1–11.

Winchester, J.A., Floyd, P.A., 1977. Geochemical discrimination of different magma series and their differentiation products using immobile elements. Chemical Geology 20, 325–343.

Xiong, X.L., Adam, J., Green, T.H., 2005. Rutile stability and rutile/meltHFSE partitioning during partial melting of hydrous basalt: implications for TTG genesis. Chemical Geology 218, 339–359.

Xu, J.F., Shinjio, R., Defant, M.J., Wang, Q., Rapp, R.P., 2002. Origin of Mesozoic adakitic intrusive rocks in the Ningzhen area of east China: partial melting of delaminated lower continental crust? Geology 30, 1111–1114.

XZBGM (Xizang Bureau of Geology and Mineral Resources), 1993. Regional Geology of Xizang Autonomous Region, China, with geologic map. Beijing: Geological Publishing House, 707 p, scale 1:1,500, 000.

Yin, A., Harrison, T.M., 2000. Geologic evolution of the Himalayan–Tibetan orogen. Annual Review of Earth and Planetary Sciences 28, 211–280. http://dx.doi.org/10.1146/annurev.earth.28.1.211.

Yin, J., Xu, J., Liu, C., Li, H., 1988. The Tibetan Plateau: regional stratigraphic context and previous work. Philosophical Transactions of the Royal Society of London, Series A 327, 5–52.

Yu, H.X., Chen, J.L., Xu, J.F., Wang, B.D., Wu, J.B., Liang, Y.H., 2011. Geochemistry and origin of Late Cretaceous (90 Ma) mineral porphyry of Balazha in mid-northern Lhasa terrane, Tibet. Acta Petrologica Sinica 27, 2011–2022 (in Chinese with English abstract).

Zhang, K.J., 2000. Cretaceous palaeogeography of Tibet and adjacent areas (China): tectonic implications. Cretaceous Research 21, 23–33.

Zhang, K.J., Xia, B.D., Wang, G.M., Li, Y.T., Ye, H.F., 2004. Early Cretaceous stratigraphy, depositional environments, sandstone provenance, and tectonic setting of central Tibet, western China. Geological Society of America Bulletin 116, 1202–1222.

Zhang, Q., Ding, L., Cai, F., Xu, X., Zhang, L., Xu, Q., Willems, H., 2012. Early Cretaceous Gangdese retroarc foreland basin evolution in the Selin Co basin, central Tibet: evidence from sedimentology and detrital zircon geochronology. Geological Society, London, Special Publications 353, 27–44.

Zhao, Z.H., Xiong, X.L., Wang, Q., Wyman, D.A., Bao, Z.W., Bai, Z.W., Qiao, Y.L., 2008. Underplating-related adakites in Xinjiang Tianshan, China. Lithos 102, 374–391.

Zhou, C.Y., Zhu, D.C., Zhao, Z.D., Xu, J.F., Wang, L.Q., Chen, H.H., Xie, L.W., Dong, G.C., Zhou, S., 2008. Petrogenesis of Daxiong Pluton in Western Gangdese, Tibet: zircon U–Pb dating and Hf isotopic constraints. Acta Petrologica Sinica 24, 348–358 (in Chinese with English abstract).

Zhu, D.C., Pan, G.T., Mo, X.X., Wang, L.Q., Zhao, Z.D., Liao, Z.L., 2006. Identification of the Mesozoic OIB-type basalts in central Qinghai–Tibetan Plateau: geochronology, geochemistry and their tectonic setting. Acta Geologica Sinica 80, 1312–1328 (in Chinese with English abstract).

Zhu, D.C., Pan, G.T., Wang, L.Q., Mo, X.X., Zhao, Z.D., Zhou, C.Y., Dong, G.C., Yuan, S.H., 2008a. Tempo-spatial variations of Mesozoic magmatic rocks in the Gangdise belt, Tibet, China, with a discussion of geodynamic setting-related issues. Geological Bulletin of China 27, 1535–1550 (in Chinese with English abstract).

Zhu, D.C., Pan, G.T., Chung, S.L., Liao, Z.L., Wang, L.Q., Li, G.M., 2008b. SHRIMP zircon age and geochemical constraints on the origin of Lower Jurassic volcanic rocks from the Yeba Formation, Southern Gangdese, South Tibet. International Geology Review 50, 442–471.

Zhu, D.C., Mo, X.X., Niu, Y.L., Zhao, Z.D., Wang, L.Q., Liu, Y.S., Wu, F.Y., 2009a. Geochemical investigation of Early Cretaceous igneous rocks along an east–west traverse throughout the central Lhasa Terrane, Tibet. Chemical Geology 268, 298–312.

Zhu, D.C., Zhao, Z.D., Pan, G.T., Lee, H.Y., Kang, Z.Q., Liao, Z.L., Wang, L.Q., Li, G.M., Dong, G.C., Liu, B., 2009b. Early cretaceous subduction-related adakite-like rocks of the Gangdese Belt, southern Tibet: products of slab melting and subsequent melt–peridotite interaction? Journal of Asian Earth Sciences 34, 298–309.

Zhu, D.C., Zhao, Z.D., Niu, Y.L., Mo, X.X., Chung, S.L., Hou, Z.Q., Wang, L.Q., Wu, F.Y., 2011. The Lhasa Terrane: record of a microcontinent and its histories of drift and growth. Earth and Planetary Science Letters 301, 241–255.

Zhu, D.C., Zhao, Z.D., Niu, Y.L., Dilek, Y., Hou, Z.Q., Mo, X.X., 2013. The origin and pre-Cenozoic evolution of the Tibetan Plateau. Gondwana Research 23, 1429–1454.